High-Resolution Gas Phase Infrared Spectroscopy of Water Clusters and Cluster Ions Using Quantum Cascade Lasers

Prospectus for Preliminary Examination

Department of Chemistry, School of Chemical Sciences

University of Illinois

Jacob T. Stewart

29 April 2011

B124 CLSL

11:00 AM

1 Introduction

Quantum cascade lasers (QCLs) are a novel type of semiconductor laser which was first invented in 1994 at Bell Labs. [1] QCLs can be designed to emit light throughout the mid-infrared and THz region of the electromagnetic spectrum by varying the underlying quantum well structure of the laser chip. The original lasers had to be operated at cryogenic temperatures in pulsed mode; however, great progress has been made and QCLs are now able to operate at room temperature with thermoelectric cooling in cw mode with output powers up to 3 W. [2]

In the short time since their introduction, QCLs have become an impressive tool for performing high-resolution spectroscopy in the mid-infrared. QCLs have been used extensively in performing trace gas analysis using known molecular absorption features, but little work has been done to utilize them in so-called "discovery spectroscopy" of previously unobserved or unresolved vibrational bands. QCLs show great promise for this type of work, with favorable characteristics for performing high-resolution spectroscopy, including narrow linewidths (<30 MHz), high optical power, and good beam quality. One of the major limitations of QCLs to this point, namely their limited tuning range, is beginning to be addressed by new technologies such as external cavity (EC) QCLs, which have been demonstrated to scan up to $\sim$200 cm^{-1}. This is a significant improvement over previous lasers, which could only scan $\sim$20 cm^{-1}. [2]

With these excellent characteristics, we are utilizing QCLs for discovery spectroscopy of interesting molecules in the mid-infrared. I have worked on constructing and testing a sensitive QCL-based spectrometer in my time at Illinois thus far. I have also begun work on acquiring and analyzing spectra of pyrene ($C_{16}H_{10}$) and small clusters of D_2O using this spectrometer. For the remainder of my time here I will continue to improve our instrument by developing an EC-QCL system for use in our lab. I also plan to acquire a rotationally-

resolved spectrum of the protonated water dimer ($H_5O_2^+$) using our improved spectrometer.

2 Progress

2.1 Development and Testing of a QCL-Based Spectrometer

In the McCall lab, we are interested in performing high-resolution spectroscopy of molecules and molecular ions of astronomical interest. One of our main goals is to acquire a rotationally-resolved, cold, gas phase infrared spectrum of buckminsterfullerene (C_{60}). In particular, we are targeting one of the four IR-active bands of C_{60} near 8.4 μm. The lead researcher on the C_{60} project has been Brian Brumfield, so I will not discuss our work toward a C_{60} spectrum in this document. I have been involved with developing a QCL-based spectrometer which is designed to observe this band. Our spectrometer is based on QCLs provided by Claire Gmachl's group at Princeton that have been specifically designed for this wavelength. [3]

The instrument is described in detail in a pair of recent publications which are attached to this paper. [4, 5] (The experimental setup is shown in Figure 1.) Our setup utilizes continuous wave-cavity ringdown spectroscopy (cw-CRDS), which is a sensitive absorption spectroscopy technique. [6] In brief, our QCL is housed in a liquid nitrogen cryostat where the temperature of the laser and the current through the laser chip (which controls the laser frequency) are controlled by computer. The light is collected by an aspheric lens and focused through an acousto-optic modulator (AOM) which acts as a fast light switch. When the AOM is on, light is sent to an optical cavity composed of two highly reflective mirrors. One of the mirrors is mounted to a piezoelectric transducer, which is driven by a function generator through a homemade piezo driver. When the cavity and laser are in resonance, light builds up in the cavity and begins to leak out of the back of the cavity onto a liquid nitrogen-cooled mercury-cadmium-telluride (MCT) detector. When the detector response reaches a designated threshold, the AOM is switched off, stopping light from going to the

cavity, and the exponential ringdown of light from the cavity is recorded by a high-speed digitizer. The time constant of this decay is inversely proportional to optical losses in the cavity, so by plotting the inverse of the time constant against the frequency of the laser, we can build up an absorption spectrum of species in the cavity. The spectrum is calibrated by simultaneously collecting reference scans of a known standard (SO_2) and measuring the frequency of the laser with a wavemeter.

To test the performance of our spectrometer, we used it to measure the ν_8 band of methylene bromide (CH_2Br_2), which had previously only been observed at low resolution at room temperature. Because of the nearly 1:1 abundance of ^{79}Br and ^{81}Br, we actually recorded overlapping spectra of three isotopologues: $CH_2{}^{79}Br_2$, $CH_2{}^{79}Br^{81}Br$, and $CH_2{}^{81}Br_2$. We were able to record $\sim$2 cm^{-1} of the rovibrational band covering the P-, Q-, and R-branches and fit the spectra to effective Hamiltonians for all three isotopologues using PGOPHER. [7] The constants from this fitting are listed in Tables 1 and 2 of the attached article "High-resolution spectroscopy of the ν_8 band of methylene bromide using a quantum cascade laser".

2.2 High-Resolution Spectroscopy of Pyrene ($C_{16}H_{10}$)

After testing the performance of our spectrometer, we moved on to a more challenging spectroscopic problem that would more closely simulate our efforts to observe C_{60}. We found that pyrene ($C_{16}H_{10}$) has a vibrational band very close in frequency to the C_{60} band that we are interested in observing. Unlike methylene bromide, pyrene needs to be heated to obtain enough gas phase sample for spectroscopy. We designed and built a high temperature source that could be used for both pyrene and C_{60}. The previous oven in use (which can be seen in Figure 4 of the attached paper from *Review of Scientific Instruments*) for this experiment had a limited sample capacity and was unable to hold liquid without having it ejected from the supersonic expansion nozzle. The new oven design (shown in Figure 2) expands the sample capacity by $\sim$7 times, which allows us to scan much further in frequency

space before we need to remove the oven from the vacuum chamber and reload sample. It also allows us to hold liquid inside of the oven, which makes it practical to heat samples above their melting point to achieve a higher vapor pressure. We attach a thermocouple to the exterior of the oven as a rough monitor of the temperature of our sample of interest. Gas phase pyrene was generated at a temperature of 155-160°C in our oven and cooled in a slit jet expansion using Ar as carrier gas.

To this point, we have been able to collect $\sim$2 cm^{-1} of the vibrational band, covering the P- and R-branches, as well as the band center (see Figure 3). Pyrene is an asymmetric top belonging to the D_{2h} point group. The vibration that we observed is a b-type band of B_{2u} symmetry, meaning it should have moderately strong wings with a weak signal near the band center, [8] as seen in Figure 3. To begin our fitting of this band, we used ground state rotational constants obtained from ultra-high-resolution laser-induced fluorescence (LIF) studies of pyrene performed by Baba et al. [9] We have successfully fit the P-branch, but saw that this led to poor results for fitting the R-branch (see Figure 4 for a plot of the residuals). We are currently investigating the cause of this discrepancy in our fit. It is likely that there are perturbations that influence this vibrational band because of the large number of atoms in pyrene. With 26 atoms, there are 72 unique vibrational modes in pyrene. Using harmonic frequencies calculated for pyrene (posted in the PAH spectral database [10]), there are 57 combination bands within $\pm$10 cm^{-1} of 1184 cm^{-1} (the approximate band center of this vibrational band). Therefore, despite symmetry restrictions for perturbations from nearby vibrational levels, it is likely that some of these bands are influencing our observed band. It is also possible that our current scans suffer from poor calibration. We are in the process of determining the cause of the poor fit and expect to finish this work in the near future.

2.3 Preliminary Spectroscopy of D_2O Clusters

In addition to work on methylene bromide and pyrene, we have also collected collected spectra of D_2O clusters generated in a supersonic jet. Water is a ubiquitous molecule, yet many of its properties are not clearly understood on a molecular level. This is due to the complex hydrogen-bond networks that develop amongst water molecules, which give water its unique properties. By obtaining high-resolution spectra of small water clusters, we can begin to unravel the interactions that occur between water molecules and build up a better theoretical understanding of bulk water. Small water clusters of D_2O have been extensively studied in the THz frequency range looking at intermolecular vibrations (see, for example, references [11, 12, 13] for the trimer, tetramer, and pentamer) but little work has been accomplished in the infrared to study the intramolecular vibrations of these clusters. There is one paper from 1998 by Paul et al. [14] that examines the O-D stretching region of the D_2O dimer with rotational resolution. This work observed the acceptor tunneling which is present in the water dimer, but did not have sufficient resolution to observe the other two tunneling pathways (donor-acceptor interchange and donor tunneling). With the high resolution provided by a slit jet expansion and a QCL, we should be able to observe these lower barrier tunneling motions.

The D_2O clusters were generated in a supersonic expansion by bubbling Ar through D_2O and expanding the mixture through a slit into our vacuum chamber. The expansion was then probed spectroscopically with our QCL spectrometer in the frequency range of the intramolecular D_2O bending mode. Our observed spectra, spanning 1195-1200 cm^{-1}, can be seen in Figure 5. This spectrum undoubtedly contains lines from many different species, such as D_2O dimer, trimer, tetramer, and $Ar{\cdot}D_2O$ cluster. We have not yet been able to assign any of the observed lines. The plan for identifying the species represented in the spectrum is outlined in the next section.

3 Future Work

3.1 Completion of Water Cluster Spectroscopy

Our next step will be to finish the work on D_2O clusters. First, we will need to identify the source of the various features that are present in the spectrum. To do this, we will use a helium expansion instead of an argon expansion to find which lines come from $Ar{\cdot}D_2O$ clusters and which lines come from pure D_2O clusters. Once we have determined which lines are from pure D_2O clusters, we will need to identify the cluster sizes for the various lines we observe. This can be done by observing the decrease in intensity of a particular line or set of lines as H_2O is added to our sample mixture. As shown by Pugliano and Saykally, [11] the reduction in intensity follows the relation:

$$\ln \frac{I_{mix}}{I_{pure}} = 2n \ln \chi_{D_2O} \tag{1}$$

Here I_{mix} is the intensity observed in a D_2O/H_2O mixture, I_{pure} is the intensity using pure D_2O, n is the cluster size (i.e., $n = 3$ for the trimer), and χ_{D_2O} is the mole fraction of D_2O in the mixture. By observing several different mixtures, we can use this relationship to find the cluster size for the observed lines.

Once we have identified the clusters present in our system, we can use the observed lines to find conditions that maximize the production of each cluster we observe and then scan our laser over as much of the vibrational band as we can reach. We can then use rotational constants from observed microwave and intermolecular THz bands as a starting point for assigning the observed lines. By assigning the vibrational bands, we will provide additional spectroscopic data to generate intermolecular potential energy surfaces for the various clusters we observe.

3.2 Development of an EC-QCL System

Our QCL spectrometer is based on relatively old QCL technology and can be improved by upgrading our laser to newer technologies that have been developed in recent years. To this end, we are collaborating with Gerard Wysocki at Princeton to develop an EC-QCL system for use in our lab. EC-QCLs have two main advantages over the Fabry-Perot (FP) QCLs that we currently use. First, EC-QCLs utilize QCL substrates which can be operated at room temperature, alleviating the need for a constant supply of liquid nitrogen for our laser. Second, EC-QCLs can scan a much wider frequency range than simple FP-QCLs, making a single laser more useful for observing a wider variety of molecules. Our current laser system can only scan $\sim$20 cm^{-1} (from 1182-1201 cm^{-1}), while a recent paper from Wysocki et al. [15] demonstrates an EC-QCL that can scan 182 cm^{-1}, showing the vast improvement in tunability that an external cavity affords.

The design of the external cavity system is shown in Figure 6 (from reference [15]). The QCL substrate is placed in an evacuated housing and attached to a thermoelectric cooler. The highly divergent light is collected and focused by a collimating lens onto a diffraction grating. The first order beam from the diffraction grating is reflected back onto the QCL, forming the external cavity, while the zero order beam is reflected from the grating onto an output mirror. The grating and output mirror are mounted on a movable stage which allows the angle and the distance of the grating from the QCL to be controlled by piezoelectric transducers. This gives fine control over the external cavity length and wavelength selection of the diffraction grating. The output mirror is mounted on the rotation stage with the diffraction grating to ensure that the laser output beam will not travel in space as the wavelength of the laser is adjusted with the diffraction grating. One of the main advantages of this setup is that different QCLs can be placed in the system to provide different wavelength ranges for spectroscopy. The only components that need to be changed are the collimating lens and the diffraction grating, which can be purchased off-the-shelf from optics supply

companies. This new laser system will allow us to pursue studies of new molecules and molecular ions, such as $H_5O_2^+$.

3.3 Rotationally-Resolved Spectroscopy of $H_5O_2^+$

3.3.1 Significance and Previous Work

While freshmen chemistry students are taught that a proton in water binds to a single water molecule to form a hydronium ion (H_3O^+), the reality is much more complex and not yet completely understood. Hydrated protons exist in large hydrogen-bonded networks with one of two main motifs at their core: the Eigen ion ($H_9O_4^+$), where an H_3O^+ core is hydrogen-bonded to three water molecules, or the Zundel ion ($H_5O_2^+$), where the proton is shared between two water molecules (see Figure 7). [16] Understanding these basic structures will give valuable insight into the structure and dynamics of hydrated protons, which are ubiquitous in chemistry. $H_5O_2^+$, in particular, is a prototypical model of aqueous proton transfer, so understanding its structure and dynamics will aid in a molecular understanding of this important process. Obtaining a rotationally-resolved spectrum of $H_5O_2^+$ will allow us to observe the tunneling splittings in this molecular ion and calculate energy barriers on the intermolecular potential energy surface.

Much work has been devoted to obtaining and understanding the vibrational spectrum of $H_5O_2^+$. Pioneering work was performed by Yeh et al. in 1989 to observe the O-H stretching vibration of gas-phase $H_5O_2^+$ near 3700 cm^{-1} using a photodissociation spectroscopy technique. [17] They followed up with a high-resolution spectrum of the same region, but this spectrum suffered from poor signal-to-noise and interference from atmospheric water, preventing assignment of the observed lines. [18] In 2003, Asmis et al. published an infrared multiphoton photodissociation (IRMPD) spectrum of $H_5O_2^+$ from 620 to 1900 cm^{-1} using a free electron laser [19], but later results using the same technique gave a much different spec-

trum. [20] Following these efforts, predissociation spectra of $H_5O_2^+$ tagged with argon and neon were obtained [21, 22], which showed a far simpler spectrum than either of the IRMPD results. The neon-tagged predissociation spectra were reproduced by a full 15-dimensional simulation [23], which was the first theoretical study to reproduce the observed doublet near 1000 cm^{-1}.

3.3.2 Proposed Research

The best spectra obtained of $H_5O_2^+$ to this point have limitations. The high-resolution work of Yeh et al. in the O-H stretching region was not assignable, while the predissociation spectra were actually measuring $H_5O_2^+$ solvated by rare gas atoms, rather than measuring the bare cluster. The presence of the rare gas atoms causes perturbations to the structure of the complex (heavy perturbations were observed for the argon-tagging experiments). The predissociation spectra were also low-resolution, not providing any fine detail in the absorption spectrum. I propose re-observing the O-H stretch region with a difference frequency laser to optimize production of $H_5O_2^+$ in a supersonic discharge source, and then using our EC-QCL system to observe the low-frequency shared proton mode near 1000 cm^{-1}. By targeting the low frequency shared proton stretch, we can address the issues that prevented assignment of the O-H stretching spectra. First, the shared proton stretch is a stronger transition than the O-H stretching modes, leading to an increase in signal-to-noise ratio. Second, this frequency region will be free from interference due to water monomer transitions. Third, the low frequency region should be clear of interference from larger protonated water clusters. Finally, the transitions observed by Yeh et al. were actually from two nearly degenerate vibrations, leading to greater complexity in the high-resolution spectrum. [18] The shared proton mode will not have this problem.

We will produce the ions using an H_2/H_2O mixture in a continuous supersonic expansion discharge source that was recently developed in our lab. [24] Using this source with cavity

ringdown spectroscopy will not allow discrimination of ions and neutrals, but the only neutrals that should be present in the expansion are H_2 and H_2O. While H_2O has transitions that will interfere with the O-H stretching region, we plan to use this spectral region to simply optimize conditions for generating $H_5O_2^+$. In the shared proton region, the only H_2O transitions are weak, so discriminating the $H_5O_2^+$ from neutrals should not be an issue. It will be more difficult to distinguish among the various cluster ions produced in the expansion. The ions present in the expansion will be H_3O^+ as well as cluster ions with more water monomers attached ($H_5O_2^+$, $H_7O_3^+$, etc.). H_3O^+ has no vibrational bands near 1000 cm^{-1}, and work by Headrick et al. [25] shows that significant absorption near 1000 cm^{-1} by clusters larger than $H_5O_2^+$ does not occur until $H_{13}O_6^+$. In experiments performed in the Saykally group at Berkeley using a corona supersonic discharge source, clusters larger than $H_9O_4^+$ could be suppressed. [26] Under these conditions we would expect little interference from other cluster ions.

4 Conclusion

I have helped to develop a sensitive QCL-based mid-infrared spectrometer, which has been tested by measuring the ν_8 band of methylene bromide. We have coupled this spectrometer with a high temperature oven to measure a C-H bending mode of pyrene near 1184 cm^{-1} in preparation for spectroscopy of C_{60}. We have also obtained preliminary spectra of the intramolecular bending mode of D_2O clusters. My future research will focus on finishing the D_2O cluster work, improving the tunability of our spectrometer by implementing an EC-QCL system, and obtaining a rotationally resolved spectrum of $H_5O_2^+$. This work will help further the development of accurate theoretical models of the molecular structure of water by directly observing tunneling splittings in small clusters and cluster ions.

References

[1] J. Faist, F. Capasso, D. L. Sivco, C. Sirtori, A. L. Hutchinson, A. Y. Cho. "Quantum cascade laser." *Science*, **264**(5158), 553 (1994).

[2] R. F. Curl, F. Capasso, C. Gmachl, A. A. Kosterev, B. McManus, R. Lewicki, M. Pusharsky, G. Wysocki, F. K. Tittel. "Quantum cascade lasers in chemical physics." *Chem. Phys. Lett.*, **487**(1-3), 1 (2010).

[3] Z. Liu, D. Wasserman, S. Howard, A. Hoffman, C. Gmachl, X. Wang, T. Tanbun-Ek, L. Cheng, F.-S. Choa. "Room-temperature continuous-wave quantum cascade lasers grown by MOCVD without lateral regrowth." *IEEE Photonics Technology Letters*, **18**(12), 1347 (2006).

[4] B. E. Brumfield, J. T. Stewart, S. L. Widicus Weaver, M. D. Escarra, S. S. Howard, C. F. Gmachl, B. J. McCall. "A quantum cascade laser cw cavity ringdown spectrometer coupled to a supersonic expansion source." *Rev. Sci. Instrum.*, **81**(6), 063102 (2010).

[5] B. E. Brumfield, J. T. Stewart, B. J. McCall. "High-resolution spectroscopy of the $\nu 8$ band of methylene bromide using a quantum cascade laser." *J. Mol. Spectrosc.*, **266**(1), 57 (2011).

[6] D. Romanini, A. A. Kachanov, N. Sadeghi, F. Stoeckel. "CW cavity ring down spectroscopy." *Chem. Phys. Lett.*, **264**(3-4), 316 (1997).

[7] C. Western. "PGOPHER, a program for simulating rotational structure, http://pgopher.chm.bris.ac.uk." (2010).

[8] J. M. Hollas. *Modern Spectroscopy.* John Wiley & Sons Ltd, Chichester, England, fourth edition (2004).

[9] M. Baba, M. Saitoh, Y. Kowaka, K. Taguma, K. Yoshida, Y. Semba, S. Kasahara, T. Yamanaka, Y. Ohshima, Y.-C. Hsu, S. H. Lin. "Vibrational and rotational structure and excited-state dynamics of pyrene." *J. Chem. Phys.*, **131**(22), 224318 (2009).

[10] C. W. Bauschlicher, C. Boersma, A. Ricca, a. L. Mattioda, J. Cami, E. Peeters, F. Sánchez de Armas, G. Puerta Saborido, D. M. Hudgins, L. J. Allamandola. "The NASA Ames polycyclic aromatic hydrocarbon infrared spectroscopic database: The computed spectra." *Astrophys. J. Suppl. Ser.*, **189**(2), 341 (2010).

[11] N. Pugliano, R. J. Saykally. "Measurement of quantum tunneling between chiral isomers of the cyclic water trimer." *Science*, **257**(5078), 1937 (1992).

[12] J. D. Cruzan, L. B. Braly, K. Liu, M. G. Brown, J. G. Loeser, R. J. Saykally. "Quantifying hydrogen bond cooperativity in water: VRT spectroscopy of the water tetramer." *Science*, **271**(5245), 59 (1996).

[13] K. Liu, M. G. Brown, J. D. Cruzan, R. J. Saykally. "Vibration-rotation tunneling spectra of the water pentamer: Structure and dynamics." *Science*, **271**(5245), 62 (1996).

[14] J. B. Paul, R. A. Provencal, R. J. Saykally. "Characterization of the $(D_2O)_2$ hydrogen-bond-acceptor antisymmetric stretch by IR cavity ringdown laser absorption spectroscopy." *J. Phys. Chem. A*, **102**(19), 3279 (1998).

[15] G. Wysocki, R. Lewicki, R. Curl, F. Tittel, L. Diehl, F. Capasso, M. Troccoli, G. Hofler, D. Bour, S. Corzine, R. Maulini, M. Giovannini, J. Faist. "Widely tunable mode-hop free external cavity quantum cascade lasers for high resolution spectroscopy and chemical sensing." *Appl. Phys. B: Lasers Opt.*, **92**(3), 305 (2008).

[16] D. Marx, M. E. Tuckerman, J. Hutter, M. Parrinello. "The nature of the hydrated excess proton in water." *Nature*, **397**(6720), 601 (1999).

[17] L. I. Yeh, M. Okumura, J. D. Myers, J. M. Price, Y. T. Lee. "Vibrational spectroscopy of the hydrated hydronium cluster ions $H_3O^+ \cdot (H_2O)_n$ (n=1, 2, 3)." *J. Chem. Phys.*, **91**(12), 7319 (1989).

[18] L. I. Yeh, Y. T. Lee, J. T. Hougen. "Vibration-rotation spectroscopy of the hydrated hydronium ions $H_5O_2^+$ and $H_9O_4^+$." *J. Mol. Spectrosc.*, **164**(2), 473 (1994).

[19] K. R. Asmis, N. L. Pivonka, G. Santambrogio, M. Brummer, C. Kaposta, D. M. Neumark, L. Woste. "Gas-phase infrared spectrum of the protonated water dimer." *Science*, **299**(5611), 1375 (2003).

[20] T. D. Fridgen, T. B. McMahon, L. MacAleese, J. Lemaire, P. Maitre. "Infrared spectrum of the protonated water dimer in the gas phase." *J. Phys. Chem. A*, **108**(42), 9008 (2004).

[21] J. M. Headrick, J. C. Bopp, M. A. Johnson. "Predissociation spectroscopy of the argon-solvated $H_5O_2^+$ 'zundel' cation in the 1000–1900 cm^{-1} region." *J. Chem. Phys.*, **121**(23), 11523 (2004).

[22] N. I. Hammer, E. G. Diken, J. R. Roscioli, M. A. Johnson, E. M. Myshakin, K. D. Jordan, A. B. McCoy, X. Huang, J. M. Bowman, S. Carter. "The vibrational predissociation spectra of the $H_5O_2^+ \cdot RG_n$ (RG = Ar,Ne) clusters: Correlation of the solvent perturbations in the free OH and shared proton transitions of the zundel ion." *J. Chem. Phys.*, **122**(24), 244301 (2005).

[23] O. Vendrell, F. Gatti, H.-D. Meyer. "Dynamics and infrared spectroscopy of the protonated water dimer." *Angew. Chem., Int. Ed.*, **46**(36), 6918 (2007).

[24] K. N. Crabtree, C. A. Kauffman, B. J. McCall. "A modular and robust continuous supersonic expansion discharge source." *Rev. Sci. Instrum.*, **81**(8), 086103 (2010).

[25] J. M. Headrick, E. G. Diken, R. S. Walters, N. I. Hammer, R. A. Christie, J. Cui, E. M. Myshakin, M. A. Duncan, M. A. Johnson, K. D. Jordan. "Spectral signatures of hydrated proton vibrations in water clusters." *Science*, **308**(5729), 1765 (2005).

[26] E. R. Keim. "Infrared laser absorption spectroscopy of fast ion beams: Cluster ions." Ph.D. thesis, University of California at Berkeley (1992).

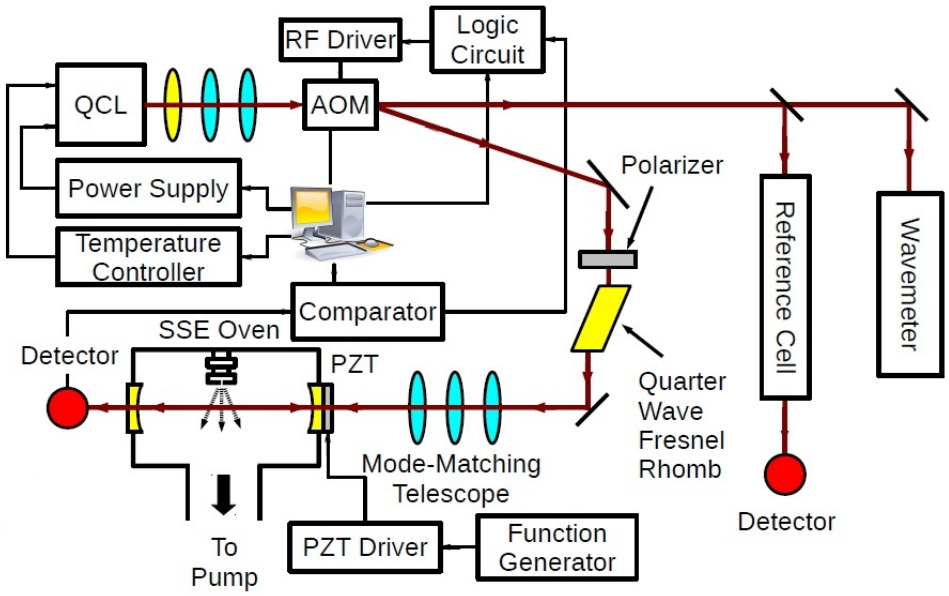

Figure 1: Experimental layout of the cavity ringdown QCL spectrometer. (QCL - quantum cascade laser, AOM - acousto-optic modulator, PZT - piezoelectric transducer, SSE - supersonic expansion)

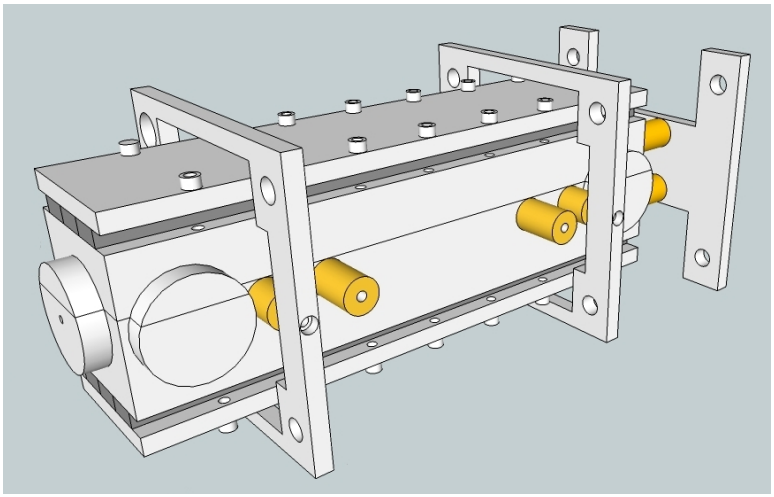

(a)

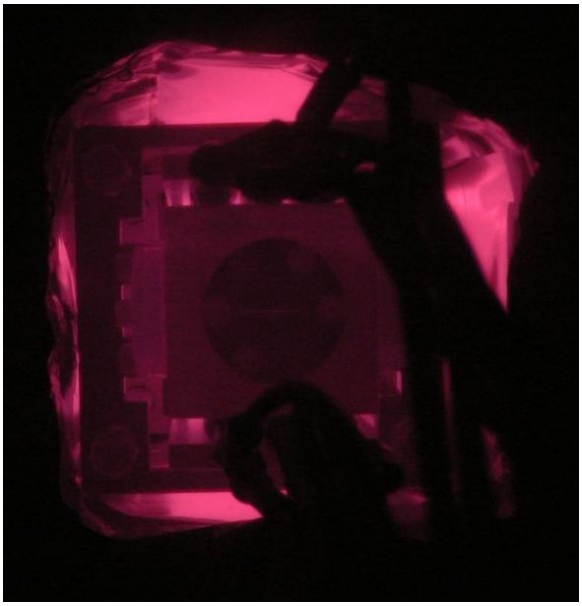

(b)

Figure 2: (a) 3D rendering of the new high temperature oven design used for pyrene spectroscopy. The yellow cylinders represent ceramic spacers, which act as thermal breaks between the oven and the supporting rods, which are rigidly attached to the vacuum chamber. Strip heaters are bolted to the top and bottom of the oven to provide heating. (b) Picture of the oven during operation at 700°C. The oven is now surrounded by an aluminum heat shield which reflects blackbody radiation back onto the oven to prevent heat loss. The pink color is due to blackbody emission from the oven. The digital camera sensor is sensitive to near-IR light, which causes the pink coloration; the oven actually glows orange at this operating temperature.

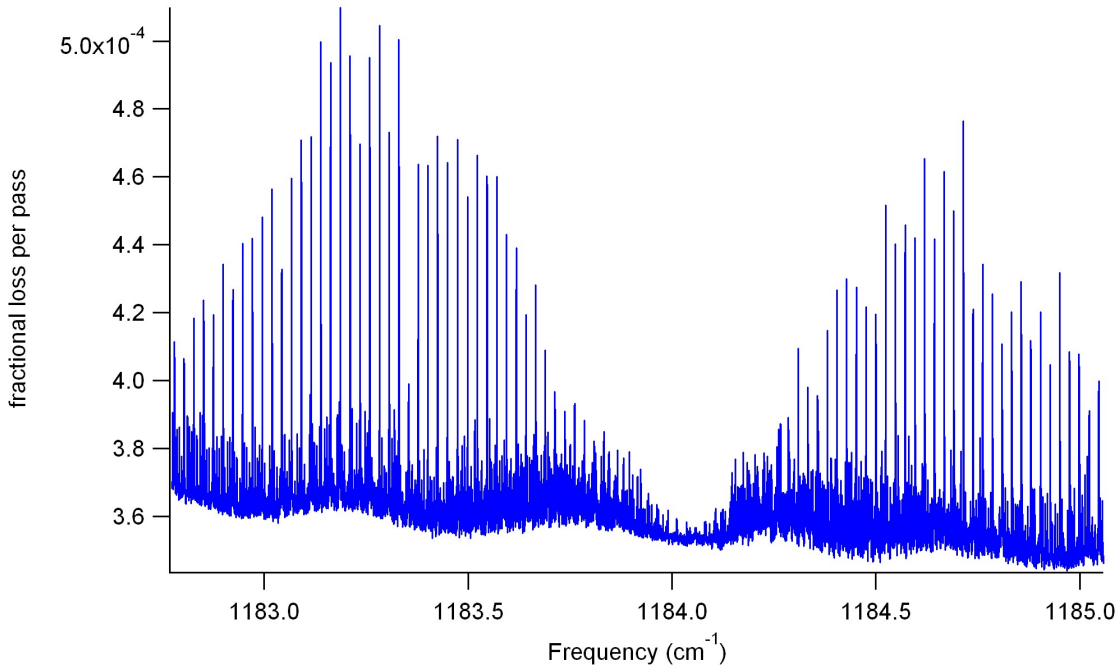

Figure 3: Rotationally-resolved vibrational spectrum of pyrene acquired using the QCL cavity ringdown spectrometer. The pyrene was heated in our high temperature oven (Figure 2) and cooled by supersonic expansion in argon. The observed lines have a linewidth of $\sim$20 MHz (FWHM)

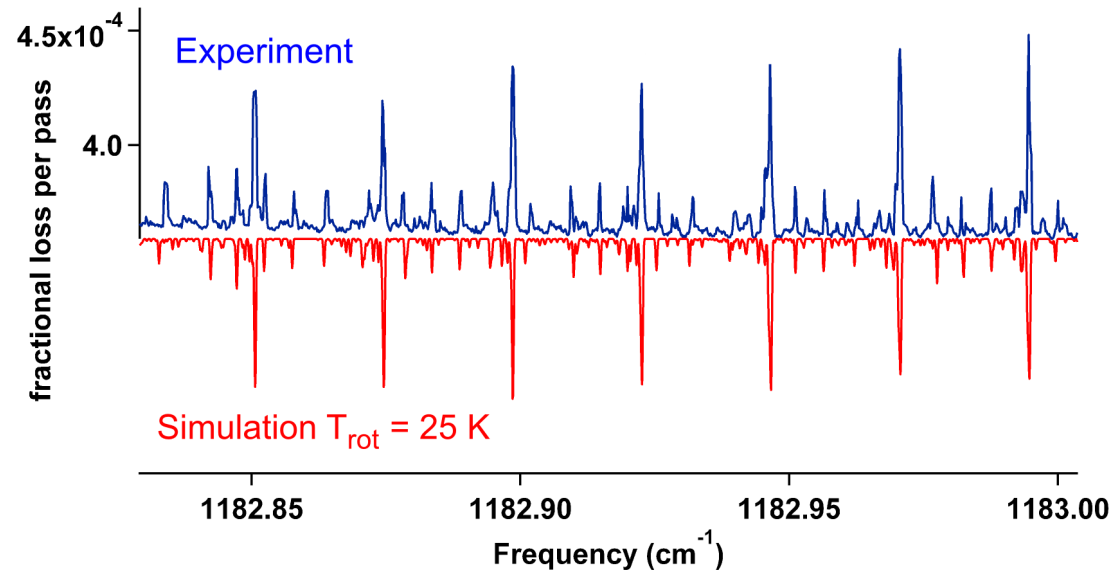

(a)

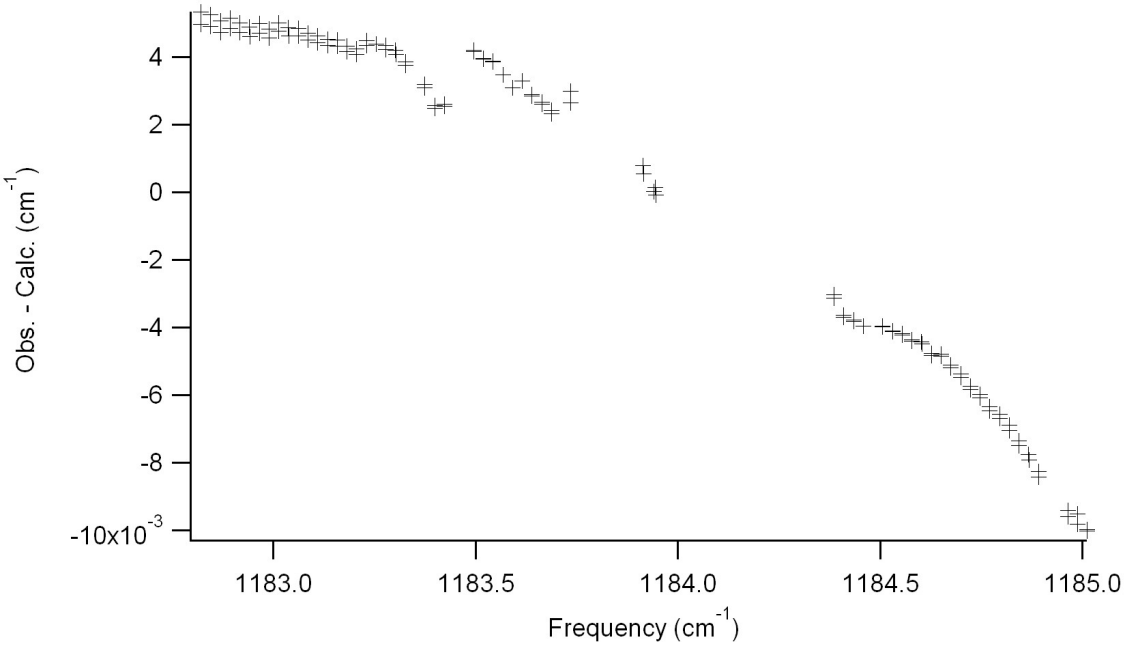

(b)

Figure 4: (a) Closeup of a portion of the P-branch with a simulation generated using PGOPHER [7] using ground state rotational constants from [9]. This simulation only assigned transitions in the P-branch, and shows the good agreement when only P-branch transitions are used. (b) A plot of the residuals when the entire band is fit. As can be seen, the agreement is poor and indicates likely perturbation of the vibrational band.

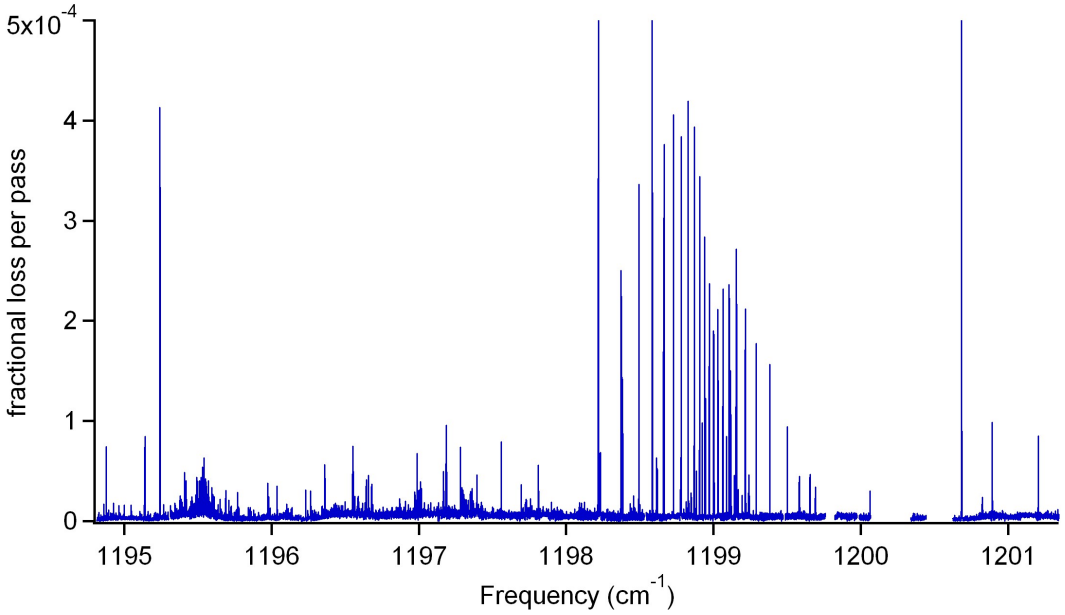

Figure 5: Collected spectra of the Ar/D_2O supersonic slit jet expansion. D_2O and HOD monomer transitions have been removed for clarity.

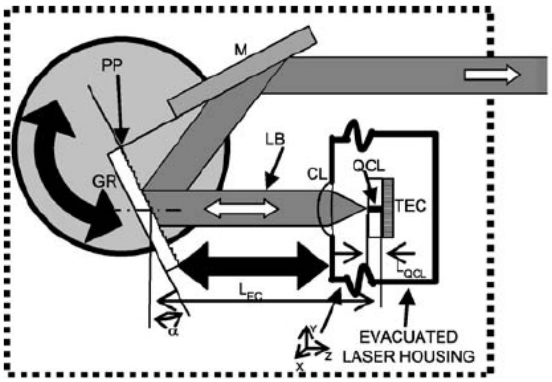

Figure 6: Design of the external cavity QCL (EC-QCL) system from [15]. (QCL - quantum cascade laser substrate, TEC - thermoelectric cooler, CL - collimating lens, LB - laser beam, GR - diffraction grating, M - output mirror, PP - pivot point of rotational movement)

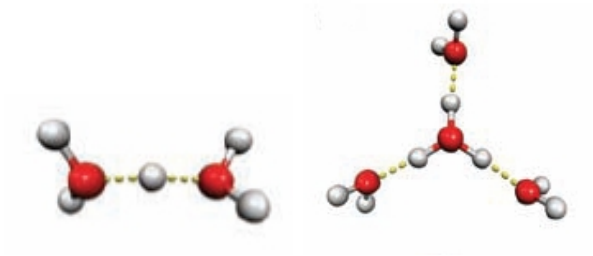

(a) (b)

Figure 7: Calculated minimum energy structures of (a) the Zundel ion ($H_5O_2^+$) and (b) the Eigen ion ($H_9O_4^+$) (from [25]).

Paper Reprints

1. "A quantum cascade laser cw cavity ringdown spectrometer coupled to a supersonic expansion source," *Review of Scientific Instruments* (2010), **81**, 063102.

2. "High-resolution spectroscopy of the ν_8 band of methylene bromide using a quantum cascade laser," *Journal of Molecular Spectroscopy* (2011), **266**, 57.

A quantum cascade laser cw cavity ringdown spectrometer coupled to a supersonic expansion source

Brian E. Brumfield,[1] Jacob T. Stewart,[1] Susanna L. Widicus Weaver,[1,a)]
Matthew D. Escarra,[2] Scott S. Howard,[2,b)] Claire F. Gmachl,[2] and Benjamin J. McCall[3]
[1]*Department of Chemistry, University of Illinois, Urbana, Illinois 61801, USA*
[2]*Department of Electrical Engineering, Princeton University, Princeton, New Jersey 08544, USA*
[3]*Departments of Chemistry and Astronomy, University of Illinois, Urbana, Illinois 61801, USA*

(Received 1 December 2009; accepted 19 April 2010; published online 8 June 2010)

A new instrument has been constructed that couples a supersonic expansion source to a continuous wave cavity ringdown spectrometer using a Fabry–Perot quantum cascade laser (QCL). The purpose of the instrument is to enable the acquisition of a cold, rotationally resolved gas phase spectrum of buckminsterfullerene (C_{60}). As a first test of the system, high resolution spectra of the ν_8 vibrational band of CH_2Br_2 have been acquired at $\sim$1197 cm^{-1}. To our knowledge, this is the first time that a vibrational band not previously recorded with rotational resolution has been acquired with a QCL-based ringdown spectrometer. 62 transitions of the three isotopologues of CH_2Br_2 were assigned and fit to effective Hamiltonians with a standard deviation of 14 MHz, which is smaller than the laser frequency step size. The spectra have a noise equivalent absorption coefficient of 1.4×10^{-8} cm^{-1}. Spectral simulations of the band indicate that the supersonic source produces rotationally cold ($\sim$7 K) molecules. © *2010 American Institute of Physics.*
[doi:10.1063/1.3427357]

I. INTRODUCTION

High resolution midinfrared (mid-IR) absorption spectroscopy has long been used as a sensitive tool for studying the fundamental bands of vibrational modes in polyatomic molecules. These modes serve as a molecule's "fingerprints," which not only provide important information about a molecule's structure and dynamics, but can also be used to detect its presence in nonlaboratory environments, including astronomical objects. Mid-IR spectroscopy is particularly valuable for studying symmetric molecules that lack permanent dipole moments and therefore cannot be studied using pure rotational spectroscopy. Examples of symmetric molecules that have been detected in astronomical objects based on high-resolution mid-IR laboratory spectroscopy include H_3^+,[1] C_2H_2,[2] CH_4,[3] and C_6H_6.[4]

The present study is motivated by the desire to search for C_{60}, which was serendipitously discovered in the laboratory during experiments designed to understand carbon star outflow chemistry[5] in astronomical environments. Of the four infrared active modes of C_{60}, only the mode near 1185 cm^{-1} is accessible for ground-based astronomical spectroscopy, as it lies in a region where the atmosphere is relatively transparent. The two major challenges in acquiring a rotationally resolved laboratory spectrum of C_{60} are developing a spectrometer with very high resolution and sensitivity near 8.5 μm, and preparing a sample of cold C_{60} in the gas phase. It should be noted that similar challenges apply to the spectroscopy of other large and symmetric carbon-bearing molecules, such as other fullerenes and polycyclic aromatic hydrocarbons. These challenges can be overcome with instruments constructed using sensitive laser direct absorption techniques coupled with high-temperature supersonic expansion sources.

Historically, there have been pulsed, and a lesser number of continuous wave (cw), laser sources available in the 8 μm region, but fewer than available in the visible and near-IR regions of the electromagnetic spectrum. Light sources such as cw optical parametric oscillators and difference frequency generation systems based on periodically poled lithium niobate (PPLN) crystals are capable of generating light spanning 2–5 μm, but progress of cw nonlinear light generation >5 μm has yet to mature to the point of offering performance comparable to those of current systems based on PPLN technology.[6] CO and CO_2 molecular gas lasers only offer partial frequency coverage from 5–6 μm and 9–11 μm, respectively.[6] Lead salt diode lasers are available in the mid-IR, but their narrow frequency coverage has limited their application.

However, the advent of quantum cascade lasers (QCLs) has enabled the fabrication of lasers with center frequencies spanning a large wavelength region in the mid-IR, using standard semiconductor materials. This is possible because the thickness of the semiconductor layers, and not their intrinsic band gap, can be varied to control the emitted photon energy.[7] Whereas lead salt diode lasers tend to have poor beam quality, generally low output powers (<1 mW), and require cryogenic cooling,[6,8] QCLs are now available with near-Gaussian beam output profiles, tens or hundreds of milliwatts of output power, and the capability to operate at room temperature. In addition to these favorable characteristics, free-running QCLs have short-term (<1 s) linewidths of

a)Present address: Department of Chemistry, Emory University, Atlanta, Georgia 30322, USA.
b)Present address: School of Applied and Engineering Physics, Cornell University, Ithaca, New York 14853, USA.

~1 MHz,[9] and submegahertz linewidths when actively frequency stabilized.[10] In comparison to nonlinear light generation methods, QCLs provide narrow spectral coverage (~20 cm^{-1}), but the development of external cavity systems and fabricated QCL arrays (providing broad coverage up to ~300 cm^{-1}) are now overcoming this difficulty.[11–13]

Consequently, QCLs are emerging as an attractive option for performing high resolution spectroscopy in the mid-IR, and have been successfully implemented into a variety of spectrometers utilizing wavelength modulation,[14–17] frequency modulation,[18] sub-Doppler Lamb dip spectroscopy,[15,19,20] integrated cavity output spectroscopy,[21–25] cw cavity ringdown spectroscopy (cw-CRDS),[26,27] and noise immune cavity enhanced optical heterodyne spectroscopy.[28] A majority of these studies were motivated as proof-of-concept implementations of cw-QCLs into previously existing techniques and/or for trace gas sensing pertinent to atmospheric science, biomedical breath analysis, and pollutant monitoring. However, two studies using QCL-based spectrometers have been carried out where a pulsed supersonic expansion was used to collect rotationally cold spectra of large molecules.[25,29]

As mentioned above, the second challenge for spectroscopy of C_{60} or related molecules is the preparation of a sample of rotationally cold gas-phase molecules. The use of supersonic expansions for cooling large molecules is a fairly mature science.[30,31] For large organic molecules, laser ablation/desorption and direct heating have been used to introduce the sample into supersonic expansions.[30–35] Using cw-CRDS with laser ablation adds the additional complication of timing the occurrence of ringdown events with the presence of sample in the supersonic jet. Though coupling cw-CRDS to pulsed sample delivery/generation has been achieved before,[36,37] given the thermal stability of C_{60} against decomposition, it is more straightforward to heat the C_{60} sample to high temperatures to provide a continuous feed of gas phase C_{60}. The high temperatures necessary to generate a significant C_{60} vapor pressure preclude the use of a pulsed supersonic expansion source, and requires a high-throughput pumping system to handle the gas load of a cw supersonic expansion source.

In the following sections, we present the experimental design and implementation of our QCL-based cw cavity ringdown spectrometer. We then present the results of our spectroscopy of a test molecule, methylene bromide (CH_2Br_2), which demonstrates the high resolution and sensitivity of our spectrometer, as well as the effectiveness of our supersonic expansion source when operated at room temperature.

II. EXPERIMENTAL

An overview of the apparatus is presented in Fig. 1. The system can be broken down into four principal parts: the quantum cascade laser (and its associated control electronics and housing), the optical layout, the data acquisition system, and the supersonic expansion source; each is described in detail below.

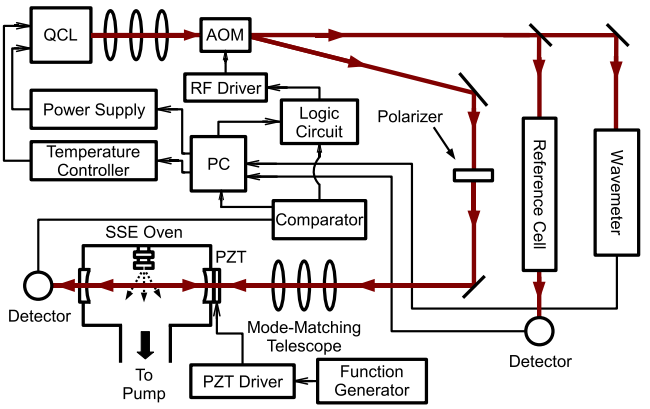

FIG. 1. (Color online) Overall experimental layout of the FP-QCL CRD spectrometer.

A. QCL

The QCLs used in the instrument have been designed and fabricated for this experiment at Princeton, with an active region design similar to that used for previously described 8.2 μm devices.[38] Unlike QCLs employing distributed feedback gratings, the lasers used in this study have short Fabry–Perot cavity lengths of ~2 mm to reduce multimode emission at higher currents (~700 mA). This approach removes the complication of adding a grating to the device, while increasing the yield of devices with the desired wavelength coverage. Shorter cavity lengths lead to a trade-off in power since the gain medium length is reduced, but there is still ample power with the shorter cavity design to carry out cavity ringdown spectroscopy.

The laser is housed inside a liquid nitrogen cooled cryostat. The cryostat was originally an unmodified Janis VPF-100, but this configuration had issues with a gradual drift in the laser pointing, and the cryostat reservoir only provided enough coolant to run for 1 h at a time. Because of these issues, significant modifications were made to the cryostat configuration.

To stabilize the laser pointing, a rigid armature was constructed, as shown in Fig. 2, and was mounted in place of one of the four cryostat windows. The copper sample mount was then disconnected from the cryostat cold plate, and held by the armature through compression of washers (outer diameter 0.25 in., inner diameter 0.115 in., thickness 0.115 in.) made of garolite (G10), a very low thermal conductivity material.[39] This was necessary to maintain reasonable thermal isolation between the cryostat outer shell and the copper submount. Thermal contact with the cold bath was achieved using a series of folded copper ribbons between the copper laser mount and the cold plate. The addition of an armature eliminated the drifting in the laser beam pointing, but because of the reduced cross-sectional area of the copper ribbons compared to the original mounting arrangement, the lowest achievable temperature with the laser operating is ~106 K. This issue has been addressed before with a different type of flexible thermal connection.[25]

In addition to the armature, the VPF-100 internal body was exchanged for a Janis Supertran FHT-ST internal body, which accepts a transfer line allowing a continuous flow of

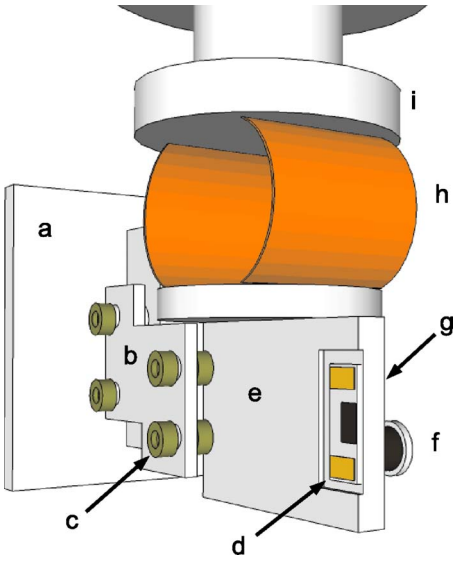

FIG. 2. (Color online) Schematic of rigid armature mount designed to eliminate laser drift as the cryostat liquid nitrogen level changed. (a) Back mounting plate; (b) armature; (c) G10 washer; (d) QCL chip; (e) copper laser mount; (f) resistive heater; (g) temperature diode (hidden from view, but adjacent to resistive heater on backside of mount); (h) copper ribbon; (i) cryostat cold plate.

liquid nitrogen to be delivered to cool the laser. This eliminated the need to refill a liquid nitrogen reservoir in hourly intervals. The liquid nitrogen is provided by an 80 L self-pressurizing liquid nitrogen Dewar (Cryofab CLPB 80-VW), which is capable of providing more than 40 h of laser run time between Dewar refills.

The laser current is provided by an ILX Lightwave (LDX-3232) power supply. To prevent inadvertent application of the wrong polarity of the applied current (which destroys the laser), a Zener diode has been added between the power supply and the laser. Additionally, the computer interface program has a high current limit that prevents a user from inadvertently applying dangerously high currents (>825 mA) to the laser. Even if this fail-safe were compromised, a built-in hardware current limit has been set on the power supply.

A Lakeshore (Model 341S) temperature controller is used in conjunction with a silicon temperature diode and a resistive heater to stabilize the temperature of the copper mount holding the QCL. The positioning of the heater and temperature sensor are shown in Fig. 2. The silicon temperature diode is positioned on the bottom of the copper mount opposite the side where the QCL is mounted, and the resistive heater is positioned adjacent to the diode on the same side of the mount. The long-term temperature stability ($\geqslant 1$ s) maintained using this configuration is $\Delta T \sim \pm 0.005$ K, as estimated by the measured laser frequency jitter using the Bristol mid-IR wavemeter and the temperature-to-frequency relationship for the laser.

To protect against accidental laser operation at temperatures that would damage the laser (>160 K), the laser current is routed through a relay in the temperature controller. The relay is programmed to close only after the cryostat temperature dips below 90 K, and to open if the laser temperature exceeds 160 K, thus preventing operation of the laser when the liquid nitrogen has run out in the self-pressurizing Dewar.

Laser frequency tuning is carried out by manipulating both the laser current start point and the temperature of the submount. By increasing the laser core temperature, either by increasing the laser current or the temperature of the laser mount, the laser output is downshifted in frequency. From empirical observations the laser has a frequency-to-current conversion of ~ 8 cm^{-1}/A, and a frequency-to-temperature conversion of ~ 0.08 cm^{-1}/K.

Using a variety of temperature and current conditions, it is possible to tune the laser in regions between 1183 and 1201 cm^{-1}. Complete coverage of the 18 cm^{-1} frequency span is not achieved due to laser mode-hops. The position of the mode-hops and tuning regions where the laser is stable can vary after an optical alignment. In regions where the laser can scan, it is possible to cover up to ~ 1 cm^{-1} before a mode-hop.

The frequency output of the QCL depends strongly on the temperature of the submount (and therefore the laser) when the laser current is brought above threshold. By monitoring the frequency output of the QCL using a cw wavemeter (Bristol 621B), it is possible to map out these temperature regions, allowing one to reproducibly bring the laser above threshold at a desired output frequency. The conditions for adjusting the laser output around 1185 cm^{-1} (C_{60}) and 1197 cm^{-1} (CH_2Br_2) can be determined through trial and error for a given optical alignment.

B. Optical layout

The divergent light output from the QCL passes through an antireflective (AR)-coated 3 in. diameter ZnSe window on the cryostat and is collimated by a 1 in. diameter AR-coated ZnSe aspheric lens (fl=2.54 cm). Light exiting the sphere is sent to a two element telescope comprised of a plano-convex BaF_2 lens (fl=50 cm) and a biconvex BaF_2 lens (fl =6.35 cm). This produces a small diameter beam that is then passed through an acousto-optic modulator (AOM). By careful alignment of the orientation of the AOM (Modulator Isomet 1207B with rf driver RFA241), and adjustment of the applied rf power, it is possible to attain a first order deflection efficiency approaching 85%. The first order beam is captured and gradually refocused using another plano-convex BaF_2 lens (fl=50 cm), and used for ringdown spectroscopy; the zero order beam is used for reference measurements.

The QCL is extremely sensitive to optical feedback, leading to issues with both the frequency coverage and the amount of mode-hop free tuning coverage achieved. To get the laser to scan stably, two approaches were utilized. First, it was necessary to tilt all of the optical components in the beam path. Second, the first order beam was passed through a holographic wire grid polarizer (Thorlabs WP25H-B). During scanning the wire grid polarizer transmission axis was kept at 20°–45° with respect to the horizontal polarization of the laser beam, corresponding to losses of 10% to 50%. In this capacity the wire grid polarizer may have served as a variable attentuator, reducing the amount of power available

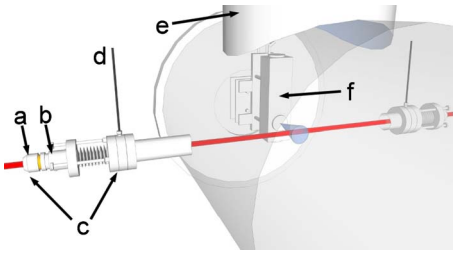

FIG. 3. (Color online) View of the chamber showing how the ringdown cavity axis is perpendicular to the expansion axis from the supersonic source. The vacuum chamber is rendered translucent in the figure. The laser beam is shown entering the mirror mount and crosses the free-jet (shown as a cone) emerging from the source. (a) Cavity ringdown mirror mount; (b) PZT; (c) kinematic mirror mount assembly; (d) N_2 purge gas line; (e) roots blower; (f) supersonic expansion source.

to back-reflect off the input ringdown mirror high reflectivity coating. The combination of these approaches reduced back reflections to the point where $\sim 1\ \mathrm{cm}^{-1}$ mode-hop free scanning is possible. A prototype optical isolator was also tested, but the amount of absorption from the optical isolator medium for a given amount of optical rotation made this approach unsuitable.

After passing through the polarizer, the first-order beam is coupled into the high finesse cavity using a three lens mode-matching telescope mounted on a meter-long dove-tail optics rail. This telescope facilitates mode-matching to the TEM_{00} mode of the ringdown cavity, and consists of a plano-convex BaF_2 (fl=20 cm), a biconcave CaF_2 (fl=−7.6 cm), and a plano-convex BaF_2 lens (fl=50 cm).

The ringdown cavity is formed from two $R(\lambda \sim 8.5\ \mu\mathrm{m}) > 0.9998$ mirrors (Laser Power Optics) with 6 m radius of curvature. The mirrors are held in homemade kinematic mounts with three precision screws to allow two-axis adjustment of their orientation. These mounts mate to ConFlat half-nipples that have been welded to the stainless steel vacuum chamber. The ringdown cavity axis is perpendicular to the supersonic expansion axis, as shown in Fig. 3. Between the vacuum chamber housing the source and the ringdown mirrors there are Swagelok connections for flowing N_2 purge gas at roughly 700 SCCM (SCCM denotes cubic centimeters per minute at STP) to protect the ringdown mirrors, and to bring the chamber up to ambient pressure without risk of particulates settling onto the mirror surfaces.

The ringdown mirror on the same side as the mode-matching telescope is mounted to a piezoelectric transducer (PZT) (Piezomechanik HPSt 150/20–15/25 VS-35) driven by a high voltage driver (Thorlabs MDT694A), with a sawtooth voltage waveform provided by a function generator. The voltage ramp applied to the PZT dithers the cavity resonances by more than one free spectral range to ensure that the laser frequency will come into resonance with the cavity at least twice during one PZT modulation cycle. Light leaking out of the cavity is focused by a short focal length plano-convex BaF_2 lens (fl=6.35 cm) onto a photoconductive mercury cadmium telluride detector (PC-MCT) (Infrared Associates MCT-9–1.0) with a 1 MHz preamplifier (Infrared Development Systems 1205). The noise equivalent power for the detector with the amplifier is $1.85 \times 10^{-12}\ \mathrm{W}/\sqrt{\mathrm{Hz}}$. The output from the MCT preamplifier is split to a high speed comparator and a 100 MHz 14-bit high speed digitizer card (National Instruments PCI-5122).

The reference arm of the optical layout relies on the zero order beam exiting the AOM. This beam is gradually refocused using a long focal length (98.7 cm) plano-convex CaF_2 lens. A ZnSe window is used as a beamsplitter, sending a small portion of the beam through a 45 cm long absorption cell, which is normally filled with SO_2 or N_2O. Light exiting the absorption cell is focused by an off-axis parabolic mirror (Janos fl=7.63 cm) onto a photovoltaic mercury zinc cadmium telluride detector (Vigo Technologies PVM-10.6) with a 1 MHz bandwidth preamplifier (VPDC-1S). The voltage output from the detector is connected to the input channel on a data acquisition board (National Instruments PCI-6221).

The remainder of the zero order beam is sent to a wavemeter. The QCL beam and the 50 μW red tracer beam from the wavemeter are initially made collinear over 1 m to align the QCL beam into the wavemeter. In this process, the QCL beam is visualized by observing the scattered mid-IR light on irises using a thermal infrared imaging camera (FLIR ThermaCam 320EX). The wavemeter has a specified accuracy of $0.001\ \mathrm{cm}^{-1}$ if it is properly aligned. However, good alignment produced a sufficient back reflection to promote laser mode-hops, and we therefore deliberately misalign the QCL beam such that the wavemeter reading is offset by $\sim 200-300$ MHz. To account for this, we calibrate the wavemeter reading using absorption lines in the direct absorption cell. The wavemeter therefore serves only as a relative frequency measurement tool, but also provides a lower accuracy real-time measure of the QCL frequency as the laser current and temperature are actively adjusted. The difference between the frequency of the first and zero order beams due to the Bragg downshifting of the first order beam is 40 MHz, and is accounted for during the frequency calibration procedure.

C. Data acquisition

During acquisition of a spectrum, the laser mount is held at a fixed temperature, while the current is stepped in small user-defined increments. The PZT is constantly dithered, bringing the ringdown cavity periodically in resonance with the laser, a scheme originally employed by Ref. 40. At each laser current, a number of ringdown transients are acquired and fit to exponential decays. Finally, direct absorption and wavemeter data are then acquired for frequency calibration. After the calibration data are collected, the laser current is then stepped. The data acquisition process is controlled by a personal computer (PC) running homemade LabWindows code, a comparator, and an AOM control circuit, as explained in more detail below.

The collection of each ringdown event begins when the cavity comes into resonance with the laser frequency, due to sweeping of the PZT, and the voltage output of the PC-MCT sharply increases. When this voltage reaches a user-defined threshold, the comparator sends out a transistor transistor logic (TTL) high pulse to the trigger input of the high speed

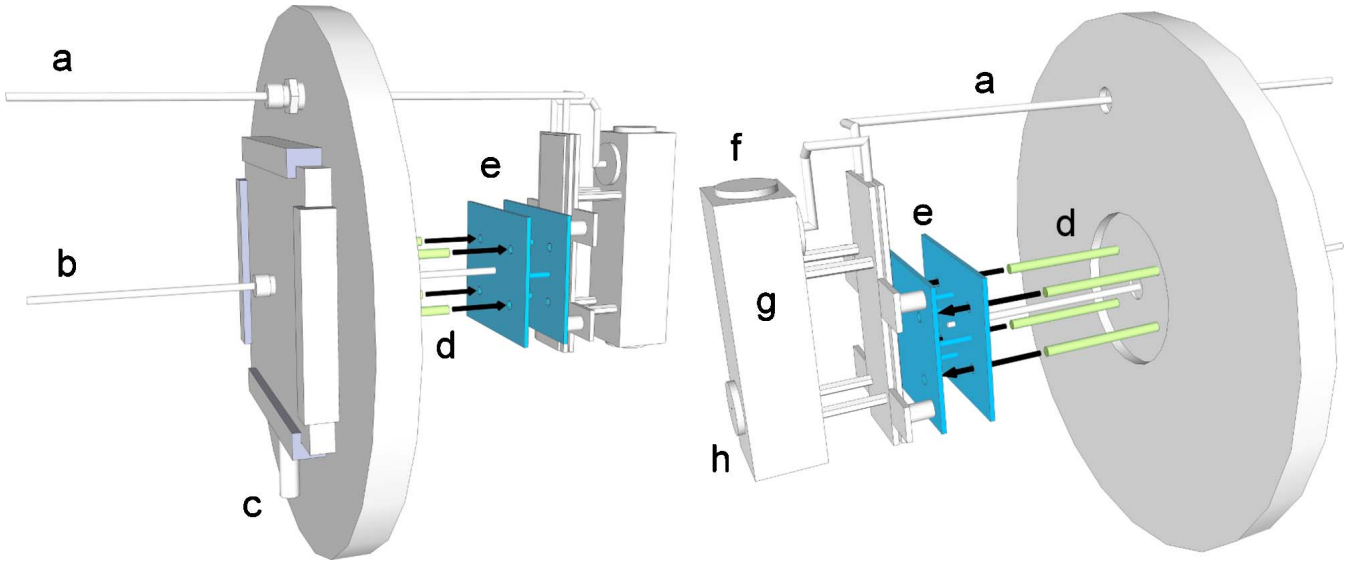

FIG. 4. (Color online) Two perspectives of the supersonic source mounted on a translatable plate attached to the back flange of the vacuum chamber. (a) Gas feedline to expansion source; (b) push-rod for adjusting nozzle distance from cavity axis; (c) height adjustment micrometer for the translatable plate; (d) rods for supporting source carriage; (e) source carriage plates; (f) Conflat blank used to seal source bore; (g) expansion source body; (h) pinhole nozzle machined into Conflat blank.

digitizer, and a TTL low pulse is sent to the AOM control circuit. The latter pulse triggers the AOM control circuit to output a TTL low pulse to the AOM rf driver, which removes the rf power from the AOM, suppressing the first order beam by −38 dB. The duration of this TTL low signal is a user set value on the comparator, and is adjusted so that one complete ringdown event can be collected without being spoiled by subsequent injection of light into the cavity. While the light going into the cavity is being attenuated, the TTL high pulse initiates data collection by the high speed digitizer. The decay event is fit in a data acquisition program using a fast algorithm that accommodates a nonzero baseline on the exponential decay.[41] Once the output time of the comparator TTL low signal has elapsed, the first order beam is turned on again, allowing the process of ringdown collection at a fixed laser current to continue.

Once the user defined number of ringdowns (typically 100) has been collected, a box-and-whiskers algorithm is used to remove the top and bottom quartile of the measured time constants. The remaining time constant values are then averaged, converted to an absorption coefficient, and recorded. The PC then sends a TTL high signal to the AOM control circuit, which overrides the signal sent from the comparator, and turns the AOM off for sufficient time to acquire calibration data. The intensity of light on the PC-MZCT detector (after passing through the direct absorption cell) is measured by the digital acquisition board, and the wavemeter is read through a universal serial bus interface. Also at this time, the laser current and temperature are read through a general purpose interface bus (GPIB) interface and recorded. Once the calibration data have been obtained, the LabWindows program uses the GPIB interface to step the laser current by a user-defined amount (typically 0.1 mA, which corresponds to ~23 MHz), and the data collection process starts again. This cycle continues until the laser current reaches the end of the desired scan range.

D. Supersonic expansion source and sample introduction

Figure 4 shows an overall view of the supersonic expansion source and its mounting in the vacuum chamber. The supersonic expansion source is composed of a stainless steel body with an attached pair of plates. The gas exits the oven body through a nozzle machined into a 1 1/3 in. ConFlat blank, which fits to a ConFlat "flange" machined into the source body (item h Fig. 4). This design makes it possible to test a variety of nozzle geometries by machining 1 1/3 in. Conflat blanks.

For the current methylene bromide jet studies a 700 μm pinhole nozzle was used. Slit nozzles were also available but not used. The slit nozzle would provide a reduction in linewidth in comparison to a pinhole nozzle,[42,43] and would provide a higher signal-to-noise (S/N) ratio for the transitions observed, but this increase is limited by the 30 MHz (0.001 cm^{-1}) linewidth of the laser. When carrying out C_{60} spectroscopy a slit nozzle geometry may be preferable because it affords better vibrational cooling due to an increase in the number of collisions early in the expansion, but this will come at the expense of an increased rotational temperature in comparison to a pinhole nozzle.[44] For flexibility it is preferable to have both nozzle types when the instrument will be used for C_{60} spectroscopy.

The source body is mounted to a carriage with two plates held in parallel (item e in Fig. 4). The parallel plates have four through-holes that line up with four rods extending from a *x*-*y* translatable flange on the back of the vacuum chamber (item d in Fig. 4). A rod is attached to the carriage and exits the chamber through an Ultra-Torr connection on the back flange (item b in Fig. 4); this allows the entire source assembly to be translated perpendicular to the ringdown cavity axis, thereby controlling the distance from the nozzle where the expansion is probed spectroscopically. The *x*-*y* translat-

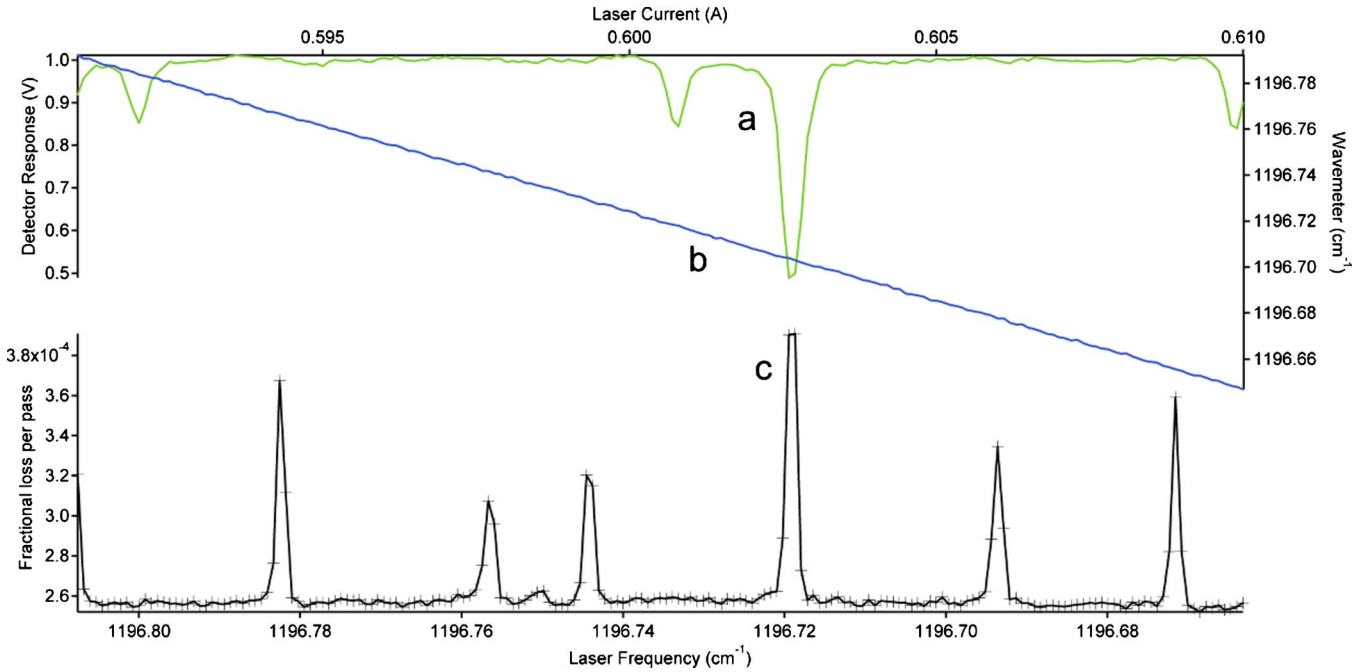

FIG. 5. (Color online) Example CH_2Br_2 scanning window of room temperature gas leaked into the chamber from 1196.792–1196.647 cm^{-1}. (a) Direct absorption scan (normalized) of SO_2. (b) Frequency readings from calibrated wavemeter. (c) Cavity ringdown spectrum of CH_2Br_2.

able flange allows adjustment of the vertical offset between the expansion and the cavity axis through the adjustment of a micrometer (item c in Fig. 4) that pushes against the translatable flange.

The supersonic source is backed by gas delivered from a mixing manifold constructed from four mass flow controllers (MKS M100B and 247D). One of the flow controllers is backed by Ar (S.J. Smith 99.95% purity) that is bubbled through methylene bromide (Aldrich 99% purity), while a second flow controller is backed with only Ar. The mole fraction of methylene bromide seeded in the expansion can then be adjusted by adjusting these two flow controllers.

While the mixing manifold and bubbler are useful for the introduction of methylene bromide to the source, the C_{60} sample introduction will be carried out differently. The C_{60} sample can be loaded directly into the hollow source bore (covered by the conflat blank labeled f in Fig. 4), which is accessible via another 1 1/3 in. ConFlat. The solid sample can be loaded in pellets that are held in place by sitting on top of a plug of quartz wool, separating the sample from the region of the bore just before the nozzle exit.

The extreme source temperatures when attempting C_{60} spectroscopy make it impractical to implement a pulsed supersonic expansion source. The large gas load generated by operating the source continuously is handled by a two-stage pumping system composed of a roots blower (Oerlikon-Leybold WS2001) and a rotary vane pump (Oerlikon-Leybold SV630). During normal flow conditions, with ~ 1 atm pressure measured after the flow controllers, and N_2 curtain gas flowing over the ringdown mirrors, the typical chamber background pressure is $\sim 20-40$ mTorr (~ 700 SCCM N_2 flow rate).

III. RESULTS AND DISCUSSION

A. Ringdown spectrometer performance

The performance of the spectrometer and the supersonic expansion source (operated at room temperature) have been evaluated using the ν_8 band of methylene bromide. Methylene bromide was selected as a test molecule because it has a vibrational band falling within the frequency coverage of our QCL. Several other molecules were considered, but methylene bromide has the advantages of being small (only five atoms), being commercially available, and whose mass is dominated by two heavy atoms making it a near prolate top with small rotational constants. The latter characteristics combine to make the rovibrational structure of the band simple, but also compact, so that it is not necessary to scan over a broad spectral window in order to estimate the rotational temperature in the expansion.

Figure 5 provides an example of one scanning window covering 0.15 cm^{-1} of the CH_2Br_2 vibrational band. This spectrum is not of a jet-cooled sample. The methylene bromide in this scan was leaked into the chamber through an open 0.25 in. inner diameter tube. Using the calibration traces, the maximum full width at half maximum (FWHM) of the spectral features seen in trace (c) is estimated to be 0.0013 cm^{-1} (40 MHz). Assuming a 30 MHz instrument linewidth, the estimated linewidth for the transition is ~ 30 MHz, which compares favorably with the 0.0011 cm^{-1} (33 MHz) FWHM Doppler broadening for a single methylene bromide line at room temperature. Between the spectral features the baseline standard deviation in the absorption coefficient is $\sim 1.4 \times 10^{-8}$ cm^{-1}, and represents the typical noise level of the system. Many spectra covering short frequency spans have been collected providing coverage from 1195.4 to 1197.15 cm^{-1}.

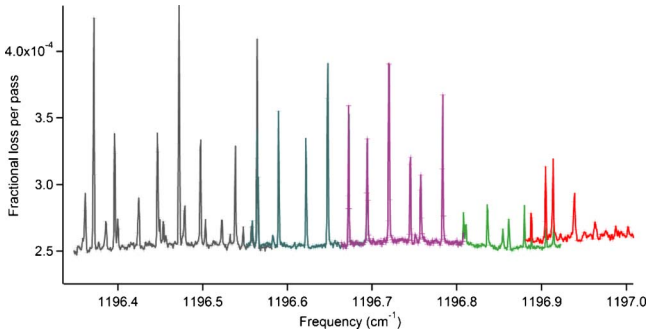

FIG. 6. (Color online) Collection of calibrated overlapped CH_2Br_2 spectra from 1196.5 to 1197.0 cm^{-1} illustrating the prominence of the strong Q-branch features from all three isotopologues. All these spectra are of room temperature gas that has been leaked into the chamber.

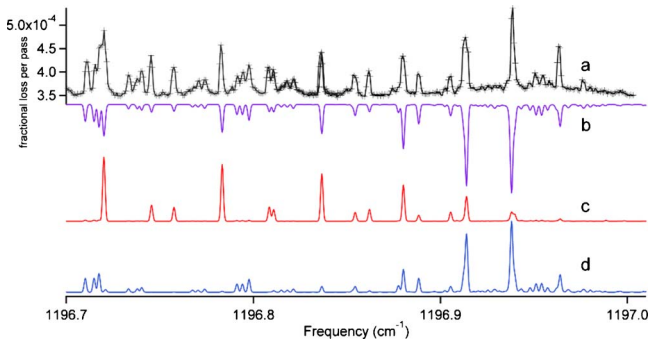

FIG. 7. (Color online) Comparison between recorded experimental spectra of CH_2Br_2 and simulated spectra with all three isotopologues at two different rotational temperatures. (a) Experimental spectra from 1196.50 to 1197.00 cm^{-1} with the nozzle 2.5 cm from the region probed, with the flow rates of the Ar only and Ar/CH_2Br_2 set to 660 and 102 SCCM, respectively; (b) simulated spectrum composed of a linearly scaled coaddition from simulations (c) and (d); (c) simulated spectrum at $T_{rot}=7$ K with a Gaussian linewidth of 0.0015 cm^{-1}; (d) simulated spectrum at $T_{rot}=300$ K with a Gaussian linewidth of 0.0015 cm^{-1}.

This is the first time that the ν_8 band of methylene bromide has been observed with sufficient resolution to reveal the rotational structure; previous spectra in the literature were acquired at low resolution, showing only the band contours of the P, Q, and R branches.[45,46] In order to evaluate the rotational cooling in the expansion, it was necessary to assign the high resolution spectrum of the jet-cooled sample.

Methylene bromide is a near-prolate asymmetric top with a Ray's asymmetry parameter of $\simeq -0.996$.[47] The CH_2 wagging motion of the ν_8 band results in a change of the dipole moment predominantly along the molecular *a*-axis, giving a parallel band structure. This leads to an easily assignable band structure, but the high abundance of two bromine isotopes provides an additional complication. The natural abundance of the ^{79}Br and ^{81}Br isotopes is roughly 1:1, and with the presence of two bromine atoms in methylene bromide a 1:2:1 abundance of $CH_2{}^{79}Br_2$, $CH_2{}^{79}Br^{81}Br$, and $CH_2{}^{81}Br_2$ isotopologues is expected in the sample. Each isotopologue will have its own parallel band, with small differences in the vibrational band center positions and rotational constants.

The detailed assignment was carried out using PGOPHER, a spectral assignment and fitting software package.[48] Ground state rotational constants from microwave spectroscopy of the $CH_2{}^{79}Br_2$,[49] $CH_2{}^{81}Br_2$,[49] and $CH_2{}^{79}Br^{81}Br$ (Ref. 50) isotopologues were used for both the ground and vibrational excited states for the initial spectral prediction.

The first set of assignments involved a progression of strong sharp spectral features seen in the spectrum of room temperature methylene bromide leaked into the chamber, as shown in Fig. 6. These features represent a series of Q-branch progressions for all three of the isotopologues. A single feature is composed of a series of tightly packed unresolved transitions sharing the same upper and lower K_a values. Because the features are narrow and not resolvable, each Q-branch feature is assigned to a single $(\nu'=1,\ J'=K_a'',\ K_a'=K_a'',\ K_c'=1) \leftarrow (\nu''=0,\ J''=K_a'',K_a'',\ K_c''=0)$ transition. In the figure, a rough 1:2:1 intensity ratio can be seen because of the isotope abundance, with the strongest features in the sequence belonging to the $CH_2{}^{79}Br^{81}Br$ isotopologue. It is important to note that not all of the spectral windows displayed in the figure were carried out with the same mole fraction of methylene bromide, so the intensities between different scanning windows cannot be directly compared.

Using these initial assignments of the Q-branches for $CH_2{}^{79}Br^{81}Br$, the experimental spectrum was fit, allowing only the band origin ν_0 and the excited state rotational constant A' to vary, with all other rotational constants constrained to values determined through pure rotational microwave spectroscopy. The Q-branch pattern resulting from fitting to these $CH_2{}^{79}Br^{81}Br$ assignments was then shifted higher in frequency to match the Q-branch progression for $CH_2{}^{79}Br_2$, and lower in frequency to assign the heavier $CH_2{}^{81}Br_2$ isotopologue. Comparison of simulations generated from fitting of the Q-branch features to the experimental spectra then enabled assignment of low J'' P-branch lines seen in the jet-cooled spectra as shown in Fig. 7.

The final results of the assignment and fitting are presented in Table I. The largest average |observed-calculated| (Avg. |o-c|) achieved for fitting to Q and P-branch transitions was 0.000 45 cm^{-1} (14 MHz). Given that the spectral features are under-sampled, that the spectra were acquired taking 0.000 77 cm^{-1} (23 MHz) frequency steps, and that only six parameters were used to fit 62 transitions, we consider this average o-c to be acceptable.

While the line frequencies of the simulations clearly match those of the experimental spectra, the simulated relative intensities (assuming a single rotational temperature) fail to match the experimental spectra acquired in the free-jet. Figure 7 highlights this by presenting two simulated spectra at T_{rot} of 300 and 7 K, traces (c) and (d), respectively. Neither simulation is a good match to the experimental spectra shown in trace (a). However, trace (b), which is a scaled linear combination of traces (c) and (d), compares better to the relative intensities of the experimental spectrum.

These results indicate that the observed spectrum is due to a combination of room temperature and rotationally cooled CH_2Br_2. Close to the band center, the Q-branch features corresponding to low K_a are dominated by the jet-cooled sample, while the room temperature contribution is negligible. Farther from the band origin (higher values of K_a), the intensity of the Q-branch features are dominated by

TABLE I. Compilation of spectroscopic constants obtained by fitting experimental spectra for all three isotopologues using PGOPHER. Only ν_0 and A' were fit, with the 1σ uncertainties from the fit provided in parentheses next to the value. A'' is taken from microwave studies, and shown for comparison to A'. The rightmost columns provide the average observed minus calculated for the fit, and the number of assigned lines for each isotopologue, respectively. The B and C rotational constants for all three isotopologues are not provided in the table because they were constrained to their values from microwave studies.

	Band constants (cm^{-1})				
	ν_0	A''	A'	Avg.|o−c|(cm^{-1})	# Assg. Lines
$CH_2{}^{79}Br_2$	1196.983 63(99)	0.868 311	0.863 451 9(22)	0.000 35	20
$CH_2{}^{79}Br^{81}Br$	1196.957 97(12)	0.867 519	0.862 664 9(28)	0.000 45	22
$CH_2{}^{81}Br_2$	1196.932 06(12)	0.866 756	0.861 910 8(23)	0.000 44	20

the room temperature background gas. The strength of the contribution from the background is not surprising because a majority of the 75 cm path length probed is chamber background gas, while the jet comprises a much smaller amount of the pathlength.

Near the band center, the relative intensities of the Q-branch features ($K_a \leq 2$) and the low-J P-branch transitions are best described by a simulation with $T_{rot}=7$ K. This illustrates the effectiveness of the expansion source for producing rotationally cold molecules, at least when operated at room temperature. The strength of the Q-branch features near the band center also serves as a feedback signal to optimize alignment overlap between the pinhole expansion source and the ringdown cavity axis.

The FWHM of the jet-cooled methylene bromide features is estimated to be ~50–60 MHz. The estimated FWHM is broader than transitions associated with the room temperature background sample. The linewidth discrepancy between the jet and background features agrees with past studies in Ar free-jets in the mid-IR, showing that the Doppler broadening associated with the expansion is greater than the room temperature Doppler broadening.[51–56] Our observed jet-cooled linewidth is comparable to, but narrower than, that seen in those previous studies.[51–56]

B. Comparison to previous QCL ringdown spectrometers

Two previous cw cavity ringdown spectrometers have been reported using QCLs.[26,27] Table II compares their single-shot standard deviations in the time constant and absorption coefficient with ours. In the two previous studies these single-shot values were determined in an empty cavity while holding the laser at a fixed frequency. The single-shot information for the current study is estimated from the measured standard deviation in the absorption coefficient (σ_α) in collected room temperature methylene bromide spectra where there are no measurable spectral features, and from the average ringdown collection rate and time constant. Close investigation of the baseline regions used did not reveal periodic fringing, as seen in the CRD study by Kosterev *et al.*[27] Because the ringdown spectra are the result of using the box-and-whiskers algorithm, the unfiltered noise level is likely worse than estimated. The σ_α was calculated using the following formula[27]

$$\sigma_\alpha = \frac{\frac{\sigma_\tau}{\langle\tau\rangle}}{c\langle\tau\rangle}, \tag{1}$$

where $\langle\tau\rangle$ is the average time constant, and σ_τ is the standard deviation of the time constant.

With a knowledge of the σ_α, and the ringdown repetition rate (f_{rep}), it is possible to calculate the instrumental sensitivity (Sy) using the following expression:[57]

$$Sy = \frac{\sigma_\alpha}{\sqrt{f_{rep}}}. \tag{2}$$

The Sy of the current study is significantly higher than the prior studies. The high Sy is related to the poor performance of our PC-MCT detector. While recording ringdown events it was necessary to start the exponential fit ~14 μs after receiving the TTL high trigger because of the long response time of the PC-MCT. This wait reduces the S/N in the portion of the decay that can be fit to a single exponential, leading to an increase in σ_τ. The comparator level also had to be set to a high voltage threshold in a trade-off between recording ringdown events with a significantly high S/N to

TABLE II. Comparison of the performance of previously reported QCL cw ringdown spectrometers with that of the current instrument.

	$\langle\tau\rangle$ (μs)	$\sigma_\tau/\langle\tau\rangle$	σ_α (cm^{-1})	f_{rep} transients (Hz)	Sy (cm^{-1} $Hz^{-1/2}$)
Paldus *et al.* (Ref. 26)	0.949	2×10^{-3}	7.2×10^{-8}	600	2.98×10^{-9}
Kosterev *et al.* (Ref. 27)	3.48	2.2×10^{-3}	2.2×10^{-8}	1600	5.50×10^{-10}
This work	~10	$\sim4.7\times10^{-2}$	1.58×10^{-7}	10	5.06×10^{-8}

improve the σ_τ, at the cost of a reduced ringdown collection rate, further impacting the instrumental sensitivity.

The manufacturer indicated that the rise time for the PC-MCT detector should be from 1 to 2 μs, which is in stark contrast to what was seen experimentally. This performance issue could in principle be due to saturation from the large amount of power directed at the detector, to issues with the AOM response, or due to a flaw with the detector itself. The power reaching the PC-MCT was reduced by two orders of magnitude, and no improvement was seen in the response of the detector to a single ringdown event. The AOM response was explored by triggering the AOM while looking at both the reference detector and PC-MCT response. The reference detector responded in 1 μs to the switching off of the AOM, while the PC-MCT took nearly 10 μs to decay to the background level.

Given these results, a PV-MCT from Kolmar Technologies (KMPV11–1-J1/AC) with a postamplifier (KA100-E2) was recently purchased as a replacement detector. This PV-MCT eliminated the long trigger delay issue, making it possible to fit after a 2.5 ms delay. Preliminary tests in an empty cavity have provided a $\sigma_\tau/\langle\tau\rangle \leq 1\times10^{-2}$, and a ringdown collection rate $\gtrsim$50 Hz. The current noise level achieved with the detector does not appear limited by the -38 dB on/off modulation ratio of the AOM, but this effect is known to cause an increase in the noise level of a cw-CRD spectrometer.[58]

IV. CONCLUSIONS

The first high-resolution spectrum of the ν_8 band of methylene bromide has been collected using a quantum cascade laser based cw cavity ringdown spectrometer, coupled to a supersonic expansion source. To our knowledge, this represents the first time that a cw ringdown QCL spectrometer has been coupled with a supersonic free-jet for the purposes of spectral discovery. The high resolution of the spectrometer has allowed the assignment and fitting of the rovibrational bands for each isotopologue, which in turn has demonstrated the effectiveness of our supersonic expansion source for producing rotationally cold molecules. The methylene bromide spectrum can now be used as a tool to optimize the overlap between the supersonic expansion and the ringdown cavity when the oven is operating at room temperature.

ACKNOWLEDGMENTS

The authors wish to thank Richard Saykally for the loan of the cryostat and the cavity ringdown mirrors used in this work, and Frank Tittel for helpful conversations regarding the frequency stability of QCLs. We also wish to acknowledge experimental assistance from Brian Siller, Brian Pohrte, and Brett McGuire. The Illinois team acknowledges financial support from NASA Laboratory Astrophysics Grant No. NNG05GE59G, the Camille and Henry Dreyfus Foundation, the David and Lucile Packard Foundation, and the University of Illinois. The Princeton team has been supported by funding from the Mid-Infrared Technologies for Health and the Environment NSF Engineering Research Center.

[1] T. R. Geballe and T. Oka, Nature (London) **384**, 334 (1996).
[2] J. H. Lacy, N. J. Evans, J. M. Achtermann, D. E. Bruce, J. F. Arens, and J. S. Carr, Astrophys. J. **342**, L43 (1989).
[3] J. H. Lacy, J. S. Carr, N. J. Evans, F. Baas, J. M. Achtermann, and J. F. Arens, Astrophys. J. **376**, 556 (1991).
[4] J. Cernicharo, A. M. Heras, A. G. G. M. Tielens, J. R. Pardo, F. Herpin, M. Guelin, and L. B. F. M. Waters, Astrophys. J. Lett. **546**, L123 (2001).
[5] H. Kroto, J. Heath, S. Obrien, R. Curl, and R. Smalley, Nature (London) **318**, 162 (1985).
[6] A. Godard, C. R. Phys. **8**, 1100 (2007).
[7] F. Capasso, C. Gmachl, D. L. Sivco, and A. Y. Cho, Phys. Today **55**(5), 34 (2002).
[8] W. Tam, I. Leonov, and Y. Xu, Rev. Sci. Instrum. **77**, 063117 (2006).
[9] D. Weidmann, L. Joly, V. Parpillon, D. Courtois, Y. Bonetti, T. Aellen, M. Beck, J. Faist, and D. Hofstetter, Opt. Lett. **28**, 704 (2003).
[10] R. M. Williams, J. F. Kelly, J. S. Hartman, S. W. Sharpe, M. S. Taubman, J. L. Hall, F. Capasso, C. Gmachl, D. L. Sivco, J. N. Baillargeon, and A. Y. Cho, Opt. Lett. **24**, 1844 (1999).
[11] G. Wysocki, R. Lewicki, R. F. Curl, F. K. Tittel, L. Diehl, F. Capasso, M. Troccoli, G. Hofler, D. Bour, S. Corzine, R. Maulini, M. Giovannini, and J. Faist, Appl. Phys. B: Lasers Opt. **92**, 305 (2008).
[12] B. G. Lee, M. A. Belkin, R. Audet, J. MacArthur, L. Diehl, C. Pflugl, F. Capasso, D. C. Oakley, D. Chapman, A. Napoleone, D. Bour, S. Corzine, G. Höfler, and J. Faist, Appl. Phys. Lett. **91**, 231101 (2007).
[13] B. Lee, H. Zhang, C. Pflugl, L. Diehl, M. Belkin, M. Fischer, A. Wittmann, J. Faist, and F. Capasso, IEEE Photonics Technol. Lett. **21**, 914 (2009).
[14] W. Weber, J. Remillard, R. Chase, J. Richert, F. Capasso, C. Gmachl, A. Hutchinson, D. Sivco, J. Baillargeon, and A. Cho, Appl. Spectrosc. **56**, 706 (2002).
[15] A. Castrillo, E. De Tommasi, L. Gianfrani, L. Sirigu, and J. Faist, Opt. Lett. **31**, 3040 (2006).
[16] B. W. M. Moeskops, S. M. Cristescu, and F. J. M. Harren, Opt. Lett. **31**, 823 (2006).
[17] G. Hancock, J. H. van Helden, R. Peverall, G. A. D. Ritchie, and R. J. Walker, Appl. Phys. Lett. **94**, 201110 (2009).
[18] S. Borri, S. Bartalini, P. De Natale, M. Inguscio, C. Gmachl, F. Capasso, D. L. Sivco, and A. Y. Cho, Appl. Phys. B: Lasers Opt. **85**, 223 (2006).
[19] J. Remillard, D. Uy, W. Weber, F. Capasso, C. Gmachl, A. Hutchinson, D. Sivco, J. Baillargeon, and A. Cho, Opt. Express **7**, 243 (2000).
[20] N. Mukherjee and C. K. N. Patel, Chem. Phys. Lett. **462**, 10 (2008).
[21] Y. Bakhirkin, A. Kosterev, C. Roller, R. Curl, and F. Tittel, Appl. Opt. **43**, 2257 (2004).
[22] Y. Bakhirkin, A. Kosterev, R. Curl, F. Tittel, D. Yarekha, L. Hvozdara, M. Giovannini, and J. Faist, Appl. Phys. B: Lasers Opt. **82**, 149 (2006).
[23] M. R. McCurdy, Y. A. Bakhirkin, and F. K. Tittel, Appl. Phys. B: Lasers Opt. **85**, 445 (2006).
[24] M. R. McCurdy, Y. Bakhirkin, G. Wysocki, and F. K. Tittel, J. Biomed. Opt. **12**, 034034 (2007).
[25] Y. Xu, X. Liu, Z. Su, R. M. Kulkarni, W. S. Tam, C. Kang, I. Leonov, and L. D'Agostino, Proc. SPIE **7222**, 722208 (2009).
[26] B. Paldus, C. Harb, T. Spence, R. Zare, C. Gmachl, F. Capasso, D. Sivco, J. Baillargeon, A. Hutchinson, and A. Cho, Opt. Lett. **25**, 666 (2000).
[27] A. A. Kosterev, A. L. Malinovsky, F. K. Tittel, C. Gmachl, F. Capasso, D. L. Sivco, J. N. Baillargeon, A. L. Hutchinson, and A. Y. Cho, Appl. Opt. **40**, 5522 (2001).
[28] M. S. Taubman, T. L. Myers, B. D. Cannon, and R. M. Williams, Spectrochim. Acta, Part A **60**, 3457 (2004).
[29] J. F. Kelly, A. Maki, T. A. Blake, and R. L. Sams, J. Mol. Spectrosc. **252**, 81 (2008).
[30] A. Amirav, U. Even, and J. Jortner, Chem. Phys. **51**, 31 (1980).
[31] A. Amirav, U. Even, and J. Jortner, Chem. Phys. Lett. **83**, 1 (1981).
[32] J. R. Cable, M. J. Tubergen, and D. H. Levy, J. Am. Chem. Soc. **109**, 6198 (1987).
[33] N. A. van Dantzig, P. Piotrowiak, and D. H. Levy, Chem. Phys. Lett. **223**, 127 (1994).
[34] J. W. Elam and D. H. Levy, J. Phys. Chem. B **102**, 8113 (1998).
[35] L. C. Snoek, T. V. Mourik, and J. P. Simons, Mol. Phys. **101**, 1239 (2003).
[36] M. Hippler and M. Quack, Chem. Phys. Lett. **314**, 273 (1999).
[37] J. Thiébaud and C. Fittschen, Appl. Phys. B: Lasers Opt. **85**, 383 (2006).
[38] Z. Liu, D. Wasserman, S. Howard, A. Hoffman, C. Gmachl, X. Wang, T. Tanbun-Ek, L. Cheng, and F.-S. Choa, IEEE Photonics Technol. Lett. **18**, 1347 (2006).

[39] S. Acharya, F. Zhou, J. Lagrone, G. Mahmood, and R. S. Bunker, J. Turbomach. **127**, 471 (2005).
[40] D. Romanini, A. Kachanov, N. Sadeghi, and F. Stoeckel, Chem. Phys. Lett. **264**, 316 (1997).
[41] D. Halmer, G. von Basum, P. Hering, and M. Murtz, Rev. Sci. Instrum. **75**, 2187 (2004).
[42] K. Veeken and J. Reuss, Appl. Phys. B: Lasers Opt. **38**, 117 (1985).
[43] C. Lovejoy and D. Nesbitt, Rev. Sci. Instrum. **58**, 807 (1987).
[44] M. Sulkes, C. Jouvet, and S. A. Rice, Chem. Phys. Lett. **87**, 515 (1982).
[45] D. Bârcă-Gălăteănu, Z. Phys. **117**, 589 (1941).
[46] *Gases and Vapours*, edited by C. Craver (The Coblentz Society, Kirkwood, 1980).
[47] D. Chadwick and D. Millen, Trans. Faraday Soc. **67**, 1539 (1971).
[48] C. Western, PGOPHER, a program for simulating rotational structure, http://pgopher.chm.bris.ac.uk (2009).
[49] R. W. Davis and M. C. L. Gerry, J. Mol. Spectrosc. **109**, 269 (1985).
[50] Y. Niide, H. Tanaka, and I. Ohkoshi, J. Mol. Spectrosc. **139**, 11 (1990).
[51] G. M. Hansford, P. B. Davies, J. Gang, and D. K. Russell, Spectrochim. Acta, Part A **53**, 1755 (1997).
[52] J. Gang, M. Pennington, D. K. Russell, F. J. Basterrechea, P. B. Davies, and G. M. Hansford, J. Opt. Soc. Am. B **11**, 184 (1994).
[53] P. Asselin, P. Soulard, L. Manceron, V. Boudon, and G. Pierre, J. Mol. Struct. **517–518**, 145 (2000).
[54] P. B. Davies, G. M. Hansford, and T. C. Killian, J. Mol. Spectrosc. **163**, 138 (1994).
[55] P. R. Brown, P. B. Davies, G. M. Hansford, and N. A. Martin, J. Mol. Spectrosc. **158**, 468 (1993).
[56] K. S. Trauth, W. A. Burns, G. Berry, and S. W. Reeve, J. Chem. Phys. **120**, 4297 (2004).
[57] *Cavity-Ringdown Spectroscopy: An Ultratrace Absorption Measurement Technique*, edited by K. Busch and M. Busch (American Chemical Society, Washington, DC, 1999).
[58] H. Huang and K. Lehmann, Appl. Phys. B: Lasers Opt. **94**, 355 (2009).

Journal of Molecular Spectroscopy 266 (2011) 57–62

Contents lists available at ScienceDirect

Journal of Molecular Spectroscopy

journal homepage: www.elsevier.com/locate/jms

High-resolution spectroscopy of the v_8 band of methylene bromide using a quantum cascade laser

Brian E. Brumfield [a], Jacob T. Stewart [a], Benjamin J. McCall [b,*]

[a] Department of Chemistry, University of Illinois, 600 South Mathews Avenue, Urbana, IL 61801, USA
[b] Departments of Chemistry and Astronomy, University of Illinois, Urbana, IL 61801, USA

ARTICLE INFO

Article history:
Received 28 December 2010
In revised form 12 February 2011

Keywords:
Methylene bromide
Quantum cascade laser
Fresnel rhomb

ABSTRACT

A continuous wave cavity ringdown spectrometer with a Fabry-Perot quantum cascade laser has been used to collect a rotationally-resolved infrared spectrum of the v_8 vibrational band of methylene bromide in a slit nozzle expansion. In our laboratory, previous observations of the vibrational band were limited by spectral coverage to only the P and Q-branches and by the 24 MHz step-size of the laser [1]. The issue of limited spectral coverage has been resolved using a Fresnel rhomb and a wire grid polarizer to protect the laser from the destabilizing effects of back-reflection from the ringdown cavity. The frequency step-size of the spectrometer has been reduced from 24 MHz to 2 MHz. With both of these instrument enhancements, we have been able to record the R-branch of the vibrational band, and can resolve many lines that were previously blended in spectra acquired using a pinhole expansion nozzle. Significant hyperfine splitting was observed for the low-J transitions in the P and R-branches. It was possible to neglect the effects of hyperfine splitting for transitions involving $J'' > 2$ in the spectral assignment, and simulations using the constants obtained by fitting to Watson's S-reduced Hamiltonian for $CH_2{}^{79}Br^{81}Br$, and the A-reduced form for $CH_2{}^{79}Br_2$ and $CH_2{}^{81}Br_2$, provide a good match to experimental spectra. A total of 297 transitions have been assigned for all three isotopologues, with a standard deviation of 0.00024 cm^{-1}($\sim$7 MHz).

1. Introduction

High-resolution gas-phase spectroscopy in the mid-infrared (mid-IR) is useful for studying the fundamental vibrational modes of molecules and molecular clusters. Lead salt diode lasers have been used to collect high-resolution gas-phase spectra of large molecules [2–6] and clusters [7–9] in supersonic expansions. Further development of lead salt diode laser spectrometers is stymied by their limited frequency coverage, low output powers, poor beam quality, and cryogenic operation.

By comparison, quantum cascade lasers (QCLs) offer several significant advantages over lead salt diode lasers. The narrow laser linewidths (<30 MHz), good beam quality, and high cw output powers ($\sim$1–100 mW) make quantum cascade lasers desirable for sensitive, high-resolution spectroscopy applications. The issue of narrow frequency coverage ($\sim$20 cm^{-1}) can be overcome by using an external cavity system [10–12]. Though there is a wealth of literature leveraging the development of QCL spectrometers towards trace gas sensing applications [13], there have been far fewer studies incorporating QCL spectrometers with supersonic expansions [1,14–16].

We are developing a continuous wave cavity ringdown (cw-CRD) spectrometer to acquire a rotationally-resolved, cold, gas-phase spectrum of a vibrational band of buckminsterfullerene (C_{60}) around 8.5 μm. In previously published work we used a supersonic expansion of methylene bromide (CH_2Br_2) seeded in argon to test the sensitivity and resolution of our QCL-based cw-CRD spectrometer [1]. During this testing several problems negatively influenced the sensitivity and resolution of the instrument. The photoconductive mercury–cadmium–telluride (PC-MCT) detector was found to have a slower response time than quoted by the manufacturer. This impaired the fitting of the ringdown decays, leading to a higher than expected noise level. Optical feedback from light rejected by the cavity induced mode-hops during scanning, and may have played a role in reducing the sensitivity of the instrument [17]. A limitation on the current step-size output by the laser power supply led to an undersampling of the methylene bromide lines.

Recently we have been able to modify the instrument to address the concerns mentioned above. To resolve the detector response time issues experienced in the previous study, we have replaced the PC-MCT detector with a photovoltaic mercury–cadmium–telluride (PV-MCT) detector. The influence of optical back-reflection has been mitigated with the addition of a Fresnel rhomb-based optical isolator. We have also decreased the current step-size of

* Corresponding author.
E-mail address: bjmccall@illinois.edu (B.J. McCall).

0022-2852/$ - see front matter © 2011 Elsevier Inc. All rights reserved.
doi:10.1016/j.jms.2011.02.013

our laser power supply, allowing us to sample methylene bromide transitions with several points per line. With our improved spectrometer, we have re-visited our earlier work on the ν_8 vibrational band of methylene bromide with better sensitivity and resolution. The following work highlights the improved instrument performance, and presents a more detailed analysis of the ν_8 vibrational band of methylene bromide for all three isotopologues.

2. Experimental

The experimental layout in this paper is similar to that presented in Brumfield et al. [1] with some modifications detailed below. We use a Fabry-Perot QCL provided by our collaborators at Princeton University.

An ILX Lightwave (LDX-3232) power supply is used to source current to the QCL. Previously, the laser current was controlled through a custom LabWindows program that communicated with the power supply over a GPIB interface. Communication over the GPIB limited the current step-size to 0.1 mA, corresponding to a frequency step-size of ~24 MHz. This limitation was overcome by using the external modulation input of the power supply. At the start of a scan the laser is brought to an initial current using the GPIB interface. A voltage output from a data acquisition (DAQ) board, which can be scanned from 0 to a maximum of 10 V, is fed into a homemade 30:1 voltage divider before entering the external modulation input. The voltage divider is used to reduce the electrical noise coupled into the cable between the DAQ board output and the power supply modulation input. During spectral acquisition the current is stepped by increasing the applied voltage to the modulation input. Using this method methylene bromide spectra were acquired with ~2 MHz frequency steps.

Infrared light exiting the QCL is collimated by a series of lenses and then passed through a Ge acousto-optic modulator (AOM). The zero order beam is sent to the reference arm of the experiment, which is comprised of a wavemeter and a 40 cm absorption cell filled with ~4 Torr of SO_2. The zero order beam is passed through the absorption cell in a triple-pass configuration to achieve a higher S/N on the SO_2 absorption features.

After sample ringdown collection, the computer sends a signal to turn off the AOM. The duration of this delay depends on whether or not a wavemeter reading will be acquired with the direct absorption cell data. For recording a frequency reading with the wavemeter, it was found that delaying 7 s after turning off the AOM provided a stable reading. This long delay is due to the limited time response of an auto-gain circuit in the wavemeter. To save time during data acquisition the wavemeter is only used every 10–50 data points. After reference data is collected the applied modulation input voltage is stepped and the process is repeated.

The first order beam passes through a wire grid polarizer (ThorLabs WP25H-B) and a ZnSe quarter wave rhomb (II-VI Infrared FRZ-8.4-.55-90-90RM). The polarizer is set to pass the horizontal polarization of the laser light. Light exiting the polarizer then passes through the quarter wave rhomb and exits as circularly polarized light. Any light that is reflected by the input ringdown mirror has the handedness of its circular polarization reversed, and upon transmission back through the rhomb is converted into vertically polarized light. The vertically polarized light is then attenuated by the ~400:1 extinction coefficient of the wire grid polarizer. This provides a potential maximum optical isolation of ~25 dB against optical back-reflection, but the achieved experimental isolation was likely less than this due to alignment errors and the actual retardation provided by the rhomb. Experimentally, the rhomb has provided sufficient protection against optical back-reflection to reduce the number of mode-hops experienced during scanning. A similar optical isolation scheme has been used with a lead salt diode laser heterodyne spectrometer [18].

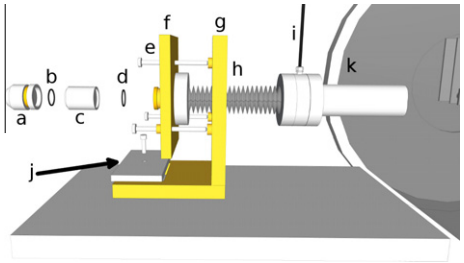

Fig. 1. Diagram showing a close-up of one of the new ringdown mounts used to form our cavity: (a) ringdown mirror in two piece aluminum holder, o-ring seal made between mirror HR surface and rightmost piece of the mirror holder, (b) o-ring for making a vacuum seal between ringdown mirror holder and piezoelectric transducer, (c) piezoelectric transducer, (d) o-ring for making a seal between the piezoelectric transducer and kinematic portion of brass mount, (e) knob adjustment screws, (f) brass kinematic plate, (g) stationary portion of brass mount, (h) metal bellows with 2 $\frac{3}{4}''$ conflat connections to the kinematic brass plate and the CF assembly connected to the half-nipple welded directly to the vacuum chamber, (i) purge gas line, (j) aluminum compression plate to secure stationary part of brass mount, (k) welded CF half-nipple extending from vacuum chamber.

After passing through the Fresnel rhomb the laser light is coupled into the ~85 cm long ringdown cavity (FSR ~ 176 MHz) using a three lens telescope. We recently acquired two new high reflectivity mirrors (Los Gatos 901-0010-8300) with 1 m radii of curvature to form our high finesse cavity. The planar side of the mirrors have an 8–12 μm broadband AR coating. New mirror mounts (shown in Fig. 1) were designed to minimize the impact of anisotropic thermal expansion of the vacuum chamber when it is under a heat load from our high-temperature oven expansion source. Each ringdown mirror is held in a two piece holder machined from aluminum. Direct contact between the piece of the aluminum holder pressed against the AR side of the mirror is cushioned by a teflon gasket. A vacuum seal is maintained on the HR side of the mirror by an o-ring seated in a groove on the second piece of the aluminum holder. This o-ring seal is not shown in Fig. 1. The mirror holder then threads onto the end of a piezoelectric transducer (PZT). A vacuum seal is formed by an o-ring (b) compressed between (a) and (c). The PZT threads onto the end of the brass kinematic plate (f). The brass kinematic plate has an o-ring groove machined onto the end, forming a vacuum seal between (c) and (f). The opposite side of the kinematic plate has a machined knife edge to create a Conflat (CF) seal with the long bellows (h). The mirror is aligned by using knob adjustment screws (e). The springs providing the restoring force holding the kinematic plate to the stationary part of the brass holder are not shown in Fig. 1. The stationary portion of the holder (g) is secured to the optics breadboard platform by compression using an aluminum plate with a through-hole for a $\frac{1}{4}$–20 screw. This made it possible to compress a sorbathane sheet between (g) and the breadboard platform. A 4″ long bellows (h) provides a flexible connection that maintains the vacuum between the ringdown mirror and the chamber by 2 $\frac{3}{4}''$ Conflat connections. The mirrors are protected from chamber dust by using the purge gas lines (i). The other ringdown mirror mount is the same as that shown in Fig. 1, but does not have the PZT (c) or o-ring (b).

We create a supersonic expansion from a 12 mm × 150 μm × 7 mm (length × width × channel depth) slit that has been machined into a 1 $\frac{1}{3}''$ conflat blank. In the previous study we used an 800 μm pinhole nozzle [1]. The backing pressure for the expansion is provided by two flow controllers, one that is fed by argon that has passed through a bubbler with methylene bromide (Aldrich 99% purity), and another drawing straight from an argon cylinder (S.J. Smith 99.95% purity). Gas exiting the flow controllers

is split to a continuous dump provided by a Welch pump and to a solenoid valve. The solenoid valve (Parker Hannifin 9S1-A1-P1-9B07) controls the flow of gas to the supersonic expansion source. When the valve is open data is taken with the jet and sample present. When the valve is closed a background spectrum is taken in the absence of the jet and sample. The delay for data acquisition between open and closed states of the valve was 2 s, and is controlled by the computer. The data was collected this way so fringing that was normally present during data collection could be subtracted. As a result of this collection process, scanning proceeded slowly at a rate of ~0.05 cm^{-1} per hour. The frequency drift of the QCL is <0.006 cm^{-1} after the laser has been on for an hour. This slow temperature drift is likely due to the temperature equilibration of the laser and cryostat mount. An example of the fringe subtraction is shown in Fig. 2.

The period and amplitude of the fringing is sensitive to the optical alignment. The frequency of the fringing falls between 400 and 600 MHz. The amplitude of the fringing varied between ~10^{-5} and 10^{-6} fractional loss per pass. All the lenses and infrared detectors in the experiment have been tilted to try to minimize etalon effects.

We have implemented a new homemade driver for the piezoelectric transducer using an audio amplifier (Samson Servo 300). Our new driver can sweep the cavity over one free spectral range at a repetition frequency greater than 250 Hz, which is a significant improvement over our previous driver's performance (<80 Hz). The ringdown collection rate varied between 50 and 200 ringdowns/s, and was dependent on the quality of the cavity alignment and the comparator trigger level setting.

Light leaking out of the cavity is focused onto a PV-MCT detector (Kolmar Technologies KMPV11-1-J1/AC). The signal from the PV-MCT is post-amplified (Kolmar Technologies KA100-E2/AC) by a factor of 20 V/V, and sent into a homemade comparator triggering circuit and a 14-bit high speed digitizer to be recorded for later processing.

When a cavity build-up event meets the comparator threshold, the comparator sends a signal to trigger the high-speed digitizer to record data. Simultaneously the computer sends out a signal to turn off the AOM so light is not being coupled into the cavity while the ringdown decay is being collected. Two sets of 100 ringdowns per point are collected per modulation voltage step because of the sample and background subtraction from the supersonic jet.

3. Results and discussion

The ν_8 band of methylene bromide was acquired from 1196.14 to 1197.92 cm^{-1}. Fig. 3 shows the experimental data collected over this range plotted with our simulation of the band. The total frequency coverage of the vibrational band was 1.78 cm^{-1}. Previously we covered 1.75 cm^{-1} of the methylene bromide band using a pinhole nozzle [1]. This prior coverage only spanned the Q and P-branches of the vibrational band because it was not possible to get reliable mode-hop free spectral coverage beyond 1197 cm^{-1} due to back-reflection induced instability. By using the Fresnel rhomb optical isolator we were able to center our spectral coverage over the band center and record portions of both the P and R-branches.

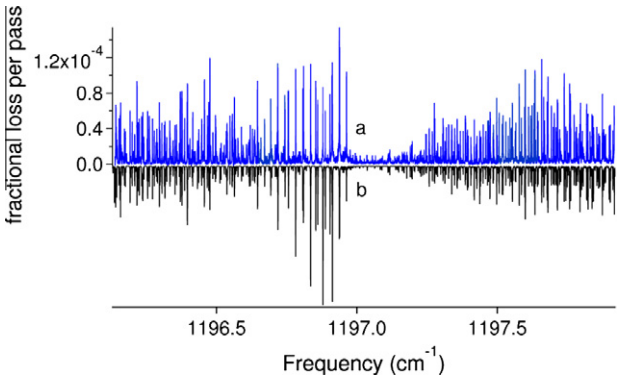

Fig. 3. Trace (a) is the experimental spectrum. Trace (b) is a simulated spectrum resulting from the assignment and fitting of the vibrational band. Trace (b) is composed of two co-added simulations created using PGOPHER [19]. One is a simulation with T_{rot} = 20 K and linewidths of 0.00045 cm^{-1} for jet-cooled methylene bromide. The second simulation is for the residual background sample contribution with T_{rot} = 300 K and linewidths of 0.0011 cm^{-1}. The 300 K simulation is scaled by a factor of 1.5 with respect to the 20 K simulation in the co-addition.

To properly simulate our experimental data, it was necessary to include a room temperature contribution because residual methylene bromide was present in the vacuum chamber. This residual sample is present because the solenoid pulse open duration is on the order of a second. It should be noted that Trace (a) in Fig. 3 is composed of many spectra spanning 0.08–0.34 cm^{-1} that were independently calibrated; Fig. 4 provides an example of one of these spectra.

The distance from the slit nozzle to the cavity axis was ~6 mm for all scans. For all scanning windows a flow rate of 75 sccm of Ar bubbled through methylene bromide and 1500 sccm of pure Ar were used. With these flow rates, when the solenoid valve was open the pressure in our vacuum chamber would rise to 70–90 mTorr.

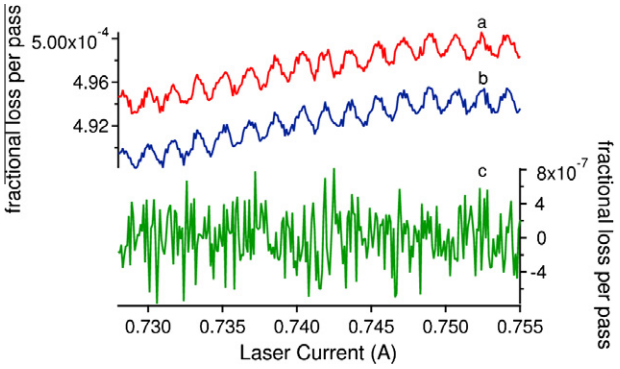

Fig. 2. Ringdown spectra of fractional loss per pass versus laser current illustrating effectiveness of background subtraction to remove fringing. There was no sample present in the expansion during this scan. Traces (a) and (b) are recorded with the jet on and off respectively. Trace (a) is offset to ease comparison with Trace (b). Trace (c) is the subtracted result from Traces (a) and (b).

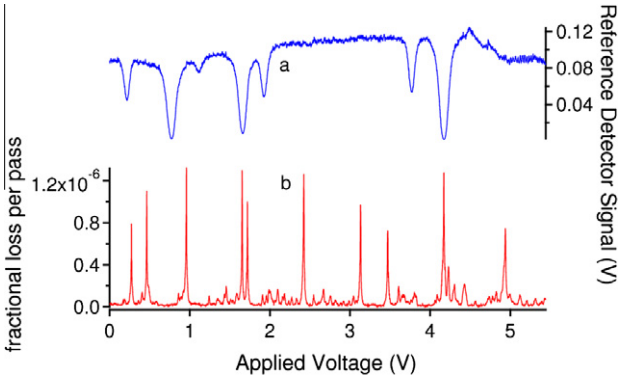

Fig. 4. Trace (a) is the signal from the direct absorption cell filled with SO_2 used for absolute frequency calibration. Trace (b) is the fringe subtracted cavity ringdown spectrum of a portion of the methylene bromide Q-branch. Both traces are plotted against the voltage applied to the modulation input on the laser power supply.

To calibrate our spectra, we utilized the wavemeter for relative frequency calibration, and SO_2 lines for absolute frequency calibration. Wavemeter data were fit to a 4th order polynomial, which was used to convert the voltage applied to the modulation input into a frequency scale. The SO_2 reference scan was then plotted against the wavemeter frequency scale. Each of the reference lines was fit to a Gaussian profile. From the Gaussian fitting a line center position calibrated to the wavemeter frequency is obtained. Because the wavemeter is intentionally misaligned, to reduce back-reflections to the QCL, there exists a frequency offset between the true frequency and that provided by the wavemeter. This offset was generally found to be between 100 and 300 MHz, and was dependent on the wavemeter alignment. To determine this offset, the difference between the wavemeter calibrated frequency and the HITRAN2008 [20] transition frequency is calculated for all the observed reference lines. All these offset values are averaged, and the resulting average is added to the wavemeter calibration, generating an absolute frequency scale for the methylene bromide spectra. The 40 MHz Bragg downshift of the AOM is also accounted for in the calibration procedure.

Overlap between individual spectra after calibration is usually good, with a difference <15 MHz. In the worst cases, the difference can be as large as 30 MHz; this is possibly limited by the uncertainty and systematic errors that exist for the SO_2 reference data in HITRAN2008 [20]. In the HITRAN2008 database, the listed uncertainty in the line positions is in the range of 3–30 MHz. In addition to these issues, some of the residuals resulting from fitting the wavemeter traces provide evidence of periodic drifting in the laser frequency less than or equal to 24 MHz. Such drifts could be explained by gradual changes in the laser temperature <0.01 K. The laser temperature control loop is not capable of correcting for such small temperature changes.

Previous work we carried out on the ν_8 band of methylene bromide was done using a pinhole nozzle expansion source [1]. Using a slit nozzle in this study provided narrower linewidths at the expense of a warmer rotational temperature. In our previous work the linewidth was around 45 MHz (0.0015 cm^{-1}), and many of the closely spaced methylene bromide lines for the three isotopologues were blended and not assignable. The narrowest transitions seen in the current work are 13.5 MHz (0.00045 cm^{-1}), which has allowed us to assign many more transitions. Assignment of the ν_8 band was initially guided by our previous assignment [1], which was refined using the new spectra. The band was then simulated using PGOPHER [19]. Methylene bromide is a near prolate top with a ground state $\kappa \sim -0.996$, and fitting was done to the A-reduced form of the asymmetric top Hamiltonian for $CH_2{}^{79}Br_2$ and $CH_2{}^{81}Br_2$, while the S-reduced form was used for $CH_2{}^{79}Br^{81}Br$. The choice of reduction was based on the availability of the ground state constants provided in microwave spectroscopy studies of methylene bromide [21,22]. The I^r representation was used for all three isotopologues. Nuclear spin statistical weights of 9:7:7:9 (J_{ee}:J_{eo}:J_{oe}:J_{oo}) were included for the $CH_2{}^{79}Br_2$ and $CH_2{}^{81}Br_2$ isotopologues. The $CH_2{}^{79}Br^{81}Br$ isotopologue lacks nuclear spin statistics because of its lower symmetry. Because of the nearly equal abundance of ^{79}Br and ^{81}Br, a 1:2:1 abundance of $CH_2{}^{79}Br_2$:$CH_2{}^{79}Br^{81}Br$:$CH_2{}^{81}Br_2$ exists in the sample. This ratio was accounted for in the simulation. Only the excited vibrational state constants ν_0, A', B', C', and $D'_K(\Delta'_K)$ were allowed to float during the fitting process, while the ground state constants were fixed to their values determined through microwave spectroscopy [21,22]. For $CH_2{}^{79}Br^{81}Br$, the value of D''_K is not known, so instead the value of $\Delta D_K = D'_K - D''_K$ was determined in the fitting process. The results of fitting the excited state spectroscopic constants are shown for $CH_2{}^{79}Br^{81}Br$ in Table 1, and for $CH_2{}^{79}Br_2$ and $CH_2{}^{81}Br_2$ in Table 2. The linelist for the assigned transitions is provided in the Supplementary material for this article.

Table 1
Listing of spectroscopic constants for the ν_8 vibrational band of $CH_2{}^{79}Br^{81}Br$ obtained by fitting to Watson's S-reduced form of the asymmetric top Hamiltonian [23]. Spectroscopic constants determined in this work are presented for each isotopologue under the "Current" column. Results of fitting from Brumfield et al. [1] are listed under the "Previous" column. The rotational constants fixed in the ground state are provided under the "Microwave" column. The units for the spectroscopic constants and the standard deviation are in wavenumbers (cm^{-1}). The 1σ uncertainties resulting from the fit are provided in parentheses at the end of each value.

	$CH_2{}^{79}Br^{81}Br$		
	ν_8=1		ν_8=0
	Previous [1]	Current	Microwave[a][22]
ν_0	1196.95797(12)	1196.957052(37)	
A	0.8626649(28)	0.8626518(25)	0.86751916(86)
B		0.0408228(16)	0.040804716(73)
C		0.0392382(14)	0.039253679(87)
ΔD_K[b]		$-2.17(22) \times 10^{-7}$	
D_J[c]			$7.75(25) \times 10^{-9}$
D_{JK}[c]			$-3.81(16) \times 10^{-7}$
d_1[c]			$-6.44(90) \times 10^{-10}$
d_2[c]			$-1.03(1.03) \times 10^{-9}$
# Assigned transitions	22	123	
Standard deviation	0.00044	0.00023	

[a] Rotational constants provided from microwave spectroscopy are for the ground state.
[b] $\Delta D_K = D'_K - D''_K$
[c] Parameter in upper state fixed to values determined from microwave spectroscopy on ground state.

The standard deviation presented in the table is defined as [19]:

$$\text{standard deviation} = \sqrt{\frac{\sum_i^{n_{obs}} (\text{obs}_i - \text{calc}_i)^2}{n_{obs} - n_{para}}} \quad (1)$$

where the total number of assigned transitions is n_{obs}, obs_i is the observed frequency position for the ith assigned transition, calc_i is the calculated frequency position for the ith transition, and n_{para} is the number of parameters floated in the least squares fitting of the spectroscopic data. The standard deviation values for the pinhole expansion work were also presented in Brumfield et al. [1], but they were mislabeled as the average |obs − calc|.

To evaluate the relative accuracy of the frequency calibration for the infrared spectra, a combination differences analysis was carried out using the infrared spectral assignments for the $CH_2{}^{79}Br^{81}Br$ isotopologue. The residuals between the 27 combination differences from the infrared data and ground state data simulated using the rotational constants from Niide et al. [22] were obtained. The standard deviation for the combination differences residuals is 0.00037 cm^{-1}, with a mean of 3.4×10^{-5} cm^{-1}. The resulting standard deviation is within a factor of 2 of the standard deviation results from the fit, and may be larger because of the smaller sample size of the combination differences in comparison to the number of assigned lines in the fit.

The increase in the number of assignments for P and R-branch transitions compared to the previous work allowed for additional excited state parameters to be fit. The failure of the current values of ν_0 to agree within their listed fit uncertainties between both studies is likely due to the use of HITRAN2004 [24] SO_2 line positions in the previous paper. A majority of the HITRAN2008 SO_2 line positions from 1197.00 to 1196.70 cm^{-1} are red-shifted by 20–30 MHz with respect to the frequency positions listed in HITRAN2004. This also explains the systematic red-shift in ν_0 compared the values from the previous study. The addition of D'_K for $CH_2{}^{79}Br_2$ and $CH_2{}^{81}Br_2$ (ΔD_K for $CH_2{}^{79}Br^{81}Br$) as a floated parameter for fitting the newest data is the reason why the values of A'

Table 2
Listing of spectroscopic constants for the ν_8 vibrational band of $CH_2{}^{79}Br_2$ and $CH_2{}^{81}Br_2$ obtained by fitting to Watson's A-reduced form of the asymmetric top Hamiltonian [23]. Spectroscopic constants determined in this work are presented for each isotopologue under the "Current" column.

	$CH_2{}^{79}Br_2$			$CH_2{}^{81}Br_2$		
	ν_8=1		ν_8=0	ν_8=1		ν_8=0
	Previous [1]	Current	Microwave[a] [21]	Previous [1]	Current	Microwave[a] [21]
ν_0	1196.98363(99)	1196.982565(56)		1196.93206(12)	1196.931350(46)	
A	0.8634519(22)	0.8634374(31)	0.868441(13)	0.8619108(23)	0.8618897(32)	0.86675642(56)
B		0.0413299(24)	0.041313137(47)		0.0403157(14)	0.040297341(27)
C		0.0397103(22)	0.039725549(53)		0.0387663(13)	0.038782329(30)
Δ_K		$1.2676(22)\times10^{-5}$	1.2922×10^{-5}[c]		$1.2667(33)\times10^{-5}$	$1.2879(15)\times10^{-5}$
Δ_J[b]			7.9321×10^{-9}[c]			$7.5662(40)\times10^{-9}$
Δ_{JK}[b]			$-3.8403(70)\times10^{-7}$			$-3.7483(20)\times10^{-7}$
δ_J[b]			$5.2279(63)\times10^{-10}$			$4.8773(70)\times10^{-10}$
δ_K[b]			3.93×10^{-8} [c]			$3.782(50)\times10^{-8}$
# Assigned transitions	20	92		20	82	
Standard deviation	0.00035	0.00027		0.00044	0.00022	

[a] Rotational constants provided from microwave work are for the ground state.
[b] Parameter in upper state fixed to values determined from microwave spectroscopy on the ground state.
[c] This parameter was constrained in the microwave work and has no reported uncertainty.

between the two studies do not agree within their listed uncertainties.

We observed complex hyperfine splitting in the low-J P and R-branch features due to the presence of the two bromine nuclei in the molecule (see Fig. 5). The presence of significant hyperfine splitting in methylene bromide was discussed in previous microwave work [25,26,22], and it was emphasized that the low-J transitions present the most complex splitting [26]. Modeling of the complex hyperfine splitting is beyond the scope of this current work, and we did not assign the $P(1)$, $R(0)$, or $R(1)$ transitions.

However, at higher J the microwave work showed that the hyperfine splitting simplified to a triplet pattern, with the peak close to the center of where a transition would be expected without the influence of hyperfine splitting [25,26]. Fig. 6 shows the occurrence of triplet patterns in a section of the R-branch spectrum for all three isotopologues. Transitions assigned with this triplet pattern are marked in the linelist included as Supplementary material to this article. Here it is assumed that the structure seen in the transition is due to hyperfine splitting, and that the asymmetry splitting of the two overlapped transitions is not resolvable given the instrument resolution. Fewer, but similar patterns are found in spectra acquired in the P-branch. In some situations a P-branch transition is seen that is broader than would be expected given the experimental linewidth, and it is likely that this broadening is the result of unresolved hyperfine splitting.

Fig. 7 shows experimental spectra acquired farther from the band center. The simulation and the experimental spectrum are in good agreement despite neglecting hyperfine interactions.

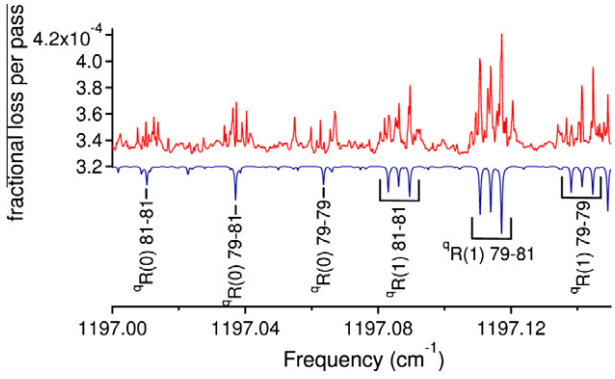

Fig. 5. The top trace is an experimental spectrum of the R-branch. The bottom trace is a section of the simulation shown in Fig. 3. The transitions in the simulation are labeled based on the isotopologue assuming no hyperfine splitting.

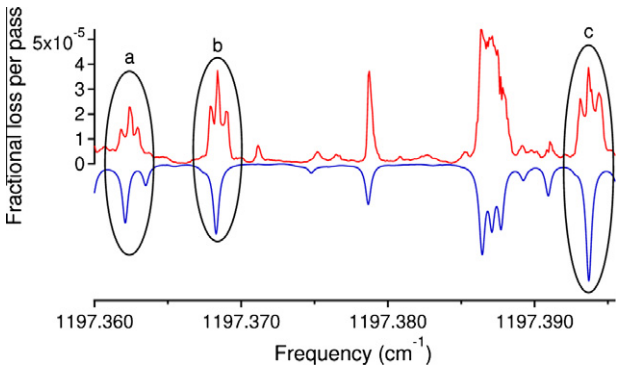

Fig. 6. The top trace is an experimental spectrum of the R-branch spanning 1197.360–1197.395 cm^{-1}. The bottom trace is a section of the simulation shown in Fig. 3. The simulated transitions paired with the triplet patterns observed in the experimental spectrum are circled. The central peak of (a) has been assigned to $^qR_{3,3}(5)$ and $^qR_{3,2}(5)$ of $CH_2{}^{81}Br_2$. The central peak of (b) has been assigned to $^qR_{2,2}(4)$ and $^qR_{2,3}(4)$ of $CH_2{}^{79}Br_2$. The central peak of (c) has been assigned to $^qR_{3,3}(5)$ and $^qR_{3,2}(4)$ of $CH_2{}^{79}Br^{81}Br$.

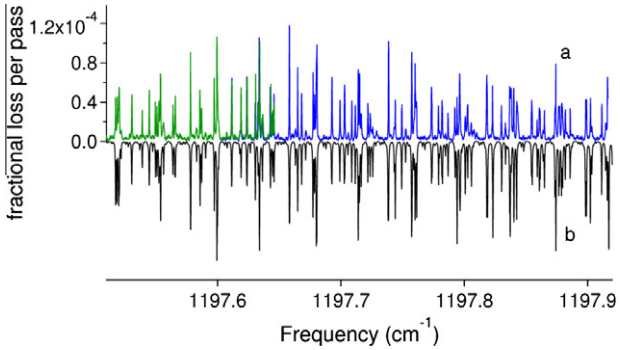

Fig. 7. Trace (a) shows two overlapped cavity ringdown spectra covering 1197.51–1197.92 cm^{-1} in the R-branch. Trace (b) is a section of the simulation shown in Fig. 3.

4. Conclusions

Recent improvements to our QCL cw-CRD spectrometer have led to an increase in the resolution and sensitivity of the instrument. As a result of these improvements, the ν_8 band of methylene

bromide was re-visited and previous spectral assignments were refined, while the total number of assignments was expanded from 62 to 297. The increase in resolution and spectral coverage revealed the presence of complex hyperfine splitting for the $P(1)$, $R(0)$, and $R(1)$ transitions that could not be assigned. Despite the absence of the low-J assignments, fitting of the bulk of the vibrational band was carried out successfully with a standard deviation of 0.00024 cm^{-1}. This study illustrates the suitability of QCL-based spectrometers for high-resolution mid-IR jet spectroscopy.

Acknowledgments

The authors wish to thank Matt Escarra and Professor Claire Gmachl from the Electrical Engineering Department at Princeton University for providing the quantum cascade lasers used in this work. Funding for this research was provided by a Packard Fellowship through the David and Lucile Packard Foundation. Jacob T. Stewart has been supported by a Robert C. and Carolyn J. Springborn Fellowship from the University of Illinois. The authors also wish to thank Professor Kevin Lehmann for suggesting the use of a Fresnel rhomb to build an optical isolator for the QCL spectrometer.

Appendix A. Supplementary data

Supplementary data associated with this article can be found, in the online version, at doi:10.1016/j.jms.2011.02.013.

Supplementary data for this article are available on ScienceDirect (www.sciencedirect.com) and as part of the Ohio State University Molecular Spectroscopy Archives (http://library.osu.edu/sites/msa/jmsa_hp.htm).

References

[1] B.E. Brumfield, J.T. Stewart, S.L.Widicus Weaver, M.D. Escarra, S.S. Howard, C.F. Gmachl, B.J. McCall, Rev. Sci. Instrum. 81 (2010) 063102.
[2] P. Asselin, P. Soulard, L. Manceron, V. Boudon, G. Pierre, J. Mol. Spectrosc. 517–518 (2000) 145–155.
[3] G.M. Hansford, P.B. Davies, J. Gang, D.K. Russell, Spectrochim. Acta Part A 53 (1997) 1755–1759.
[4] P.R. Brown, P.B. Davies, G.M. Hansford, N.A. Martin, J. Mol. Spectrosc. 158 (1993) 468–478.
[5] P.B. Davies, G.M. Hansford, T.C. Killian, J. Mol. Spectrosc. 163 (1994) 138–158.
[6] J. Gang, M. Pennington, D.K. Russell, F.J. Basterrechea, P.B. Davies, G.M. Hansford, J. Opt. Soc. Am. B 11 (1994) 184–190.
[7] H. Qian, W.A. Herrebout, B.J. Howard, Mol. Phys. 91 (1997) 689–696.
[8] M. Wangler, D. Roth, I. Pak, G. Winnewisser, P. Wormer, A. van der Avoird, J. Mol. Spectrosc. 222 (2003) 109–120.
[9] G. Winnewisser, T. Drascher, T. Giesen, I. Pak, F. Schiilling, R. Schieder, Spectrochim. Acta Part A 55 (1999) 2121–2142.
[10] B.G. Lee, M.A. Belkin, R. Audet, J. MacArthur, L. Diehl, C. Pflugl, F. Capasso, D.C. Oakley, D. Chapman, A. Napoleone, D. Bour, S. Corzine, G. Hofler, J. Faist, Appl. Phys. Lett. 91 (2007) 231101–231103.
[11] G. Wysocki, R. Lewicki, R. Curl, F. Tittel, L. Diehl, F. Capasso, M. Troccoli, G. Hofler, D. Bour, S. Corzine, R. Maulini, M. Giovannini, J. Faist, Appl. Phys. B: Lasers Opt. 92 (2008) 305–311.
[12] R. Maulini, I. Dunayevskiy, A. Lyakh, A. Tsekoun, C. Patel, L. Diehl, C. Pflugl, F. Capasso, Electron. Lett. 45 (2009) 107–108.
[13] A. Kosterev, G. Wysocki, Y. Bakhirkin, S. So, R. Lewicki, M. Fraser, F. Tittel, R. Curl, Appl. Phys. B: Lasers Opt. 90 (2008) 165–176.
[14] J.F. Kelly, A. Maki, T.A. Blake, R.L. Sams, J. Mol. Spectrosc. 252 (2008) 81–89.
[15] Y. Xu, X. Liu, Z. Su, R.M. Kulkarni, W.S. Tam, C. Kang, I. Leonov, L. D'Agostino, Proc. SPIE 7222 (2009) 722208–722211.
[16] J. Krieg, V. Lutter, F.X. Hardy, S. Schlemmer, T.F. Giesen, J. Chem. Phys. 132 (2010) 224306.
[17] G.N. Rao, A. Karpf, Appl. Opt. 49 (2010) 4906–4914.
[18] R. Schieder, Infrared Phys. Technol. 35 (1994) 477–486.
[19] C.M. Western, Pgopher, a program for simulating rotational structure, 2010. <http://pgopher.chm.bris.ac.uk>.
[20] L. Rothman, I. Gordon, A. Barbe, D. Benner, P. Bernath, M. Birk, V. Boudon, L. Brown, A. Campargue, J.-P. Champion, K. Chance, L. Coudert, V. Dana, V. Devi, S. Fally, J. Flaud, R. Gamache, A. Goldman, I. Jacquemart, D. Kleiner, N. Lacome, W. Lafferty, J. Mandin, S. Massie, S. Mikhailenko, C. Miller, N. Moazzen-Ahmadi, O. Naumenko, A. Nikitin, J. Orphal, V. Perevalov, A. Perrin, A. Predoi-Cross, C. Rinsland, M. Rotger, M. Šimečková, M. Smith, K. Sung, S. Tashkun, J. Tennyson, R. Toth, A. Vandaele, J. Vander Auwera, J. Quant. Spectrosc. Radiat. Transfer 110 (2009) 533–572.
[21] R.W. Davis, M.C.L. Gerry, J. Mol. Spectrosc. 109 (1985) 269–282.
[22] Y. Niide, H. Tanaka, I. Ohkoshi, J. Mol. Spectrosc. 139 (1990) 11–29.
[23] J. Watson, Vibrational Spectra and Structure, vol. 6, Elsevier, 1977, pp. 2–89.
[24] L. Rothman, D. Jacquemart, A. Barbe, D. Chris Benner, M. Birk, L. Brown, M. Carleer, C. Chackerian Jr., K. Chance, L. Coudert, V. Dana, V. Devi, J.-M. Flaud, R. Gamache, A. Goldman, J.-M. Hartmann, K. Jucks, A. Maki, J.-Y. Mandin, S. Massie, J. Orphal, A. Perrin, C. Rinsland, M. Smith, J. Tennyson, R. Tolchenov, R. Toth, J. Vander Auwera, P. Varanasi, G. Wagner, J. Quant. Spectrosc. Radiat. Transfer 96 (2005) 139–204.
[25] D. Chadwick, D.J. Millen, Trans. Faraday Soc. 67 (1971) 1539–1550.
[26] D. Chadwick, D.J. Millen, Trans. Faraday Soc. 67 (1971) 1551–1568.